Geoscience Frontiers 13 (2022) 101167

HOSTED BY

Contents lists available at ScienceDirect

Geoscience Frontiers

journal homepage: www.elsevier.com/locate/gsf

Research Paper

Isotopic and geochemical constraints for a Paleoproterozoic accretionary orogen in the Borborema Province, NE Brazil: Implications for reconstructing Nuna/Columbia

Lauro Cézar M. de Lira Santos [a,*], Geysson A. Lages [b], Fabrício A. Caxito [c], Elton L. Dantas [d], Peter A. Cawood [e], Haroldo M. Lima [f], Felipe J. da Cruz Lima [b]

[a] Departamento de Geologia, Universidade Federal de Pernambuco, Av. da Arquitetura, Cidade Universitária, Recife, PE, Brazil
[b] Serviço Geológico do Brasil - CPRM, Av. Sul, Afogados, Recife, PE, Brazil
[c] CPMTC, Instituto de Geociências, Universidade Federal de Minas Gerais, Av. Pres. Antônio Carlos, Pampulha, Belo Horizonte, MG, Brazil
[d] Instituto de Geociências, Universidade de Brasília, Campus Universitário Darcy Ribeiro, Asa Norte, Brasília, DF, Brazil
[e] School of Earth, Atmosphere and Environment, Monash University, Wellington Rd, Clayton, VIC 3800, Australia
[f] Departamento de Geologia, Universidade Federal do Ceará, Campus do Pici, Parquelândia, Fortaleza, CE, Brazil

ARTICLE INFO

Article history:
Received 26 August 2020
Revised 25 January 2021
Accepted 28 January 2021
Available online 08 February 2021

Keywords:
Paleoproterozoic accretionary-collisional event
Early orogenic and *syn*-collisional magmatism
Paleoproterozoic inlier within West Gondwana
Nuna/Columbia Supercontinent

ABSTRACT

The Alto Moxotó Terrane of the Borborema Province presents a wide exposure of Paleoproterozoic crust, but unlike other continental blocks of South America, its orogenic history is strongly obliterated by late Neoproterozoic deformation. New isotopic and geochemical studies were conducted in mafic-ultramafic (Fazenda Carmo Suite) and granitic-gneissic rocks (Riacho do Navio Suite) within the terrane. The former present zircon U-Pb crystallization ages at ca. 2.13 Ga, whereas Sm-Nd data suggests a juvenile origin via melting of early Paleoproterozoic to Archean peridotitic sources. Geochemical data for these rocks are compatible with tholeiitic magmas with some degree of crustal contamination and trace element distribution points to a continental-arc related setting interpreted as remnants of the early stages of subduction. In contrast, the Riacho do Navio Suite was emplaced at ca. 2.08 Ga and has highly negative $\varepsilon_{Nd}(t)$ values indicating crustal reworking. The suite displays calc-alkali to alkali-calcic and ferroan geochemical signatures compatible with Cordilleran magmas. In addition, trace-element distribution as well as discriminant diagrams suggest that the precursor magmas were generated during the later stages of a continental arc or in a *syn*-collisional setting. Based on our results, we suggest that the studied units might represent missing pieces of a Paleoproterozoic accretionary orogen that formed the crustal framework of the Alto Moxotó Terrane, and that this represents a block associated with assembly of the Nuna/Columbia supercontinent, which is now largely hidden within the Neoproterozoic orogenic belts of West Gondwana.

1. Introduction

Accretionary orogens have played a major role in lithospheric processes throughout Earth history and involve the development of large-scale mountain chains, which have provided resources for the hydrosphere, atmosphere and biosphere (Ganade de Araujo et al., 2014a, 2014b; Cawood et al., 2018). Unlike the well-known Pangaea supercontinent that was assembled and broke-up during the Phanerozoic (ca. 540–250 Ma), paleogeographic reconstructions for the Precambrian lithosphere are less well constrained due to major gaps in the rock record.

Compilation of U-Pb, Sm-Nd and Hf data from different sources have been considered proxies for ancient supercontinent assembly events (e.g., Hawkesworth et al., 2017), which are closely associated with the crustal growth record (Nance and Murphy, 2013; Condie et al., 2015). Integration of paleomagnetic, geochronological and geochemical data has suggested that widespread subduction-collisional episodes took place during the 2.2–2.0 Ga interval, resulting in the assembly of the Paleoproterozoic Columbia/Nuna supercontinent, and its later fragmentation starting from around ca. 1.6 Ga (Zhao et al., 2002, 2004; Reddy and Evans, 2009; Meert and Santosh, 2017).

* Corresponding author.
E-mail address: lauro.lsantos@ufpe.br (L.C.M. de Lira Santos).

https://doi.org/10.1016/j.gsf.2021.101167

In West Gondwana, Paleoproterozoic orogenic belts are abundant in its major cratons including the São Francisco-Congo and the São-Luis West Africa paleocontinents (e.g., De Waele et al., 2008; Pedreira and De Waele, 2008; Bruno et al., 2020; Caxito et al., 2020). Within these blocks, evidence of crustal accretion is strongly based on preserved eclogitic-granulitic belts (i.e. suture zones), dismembered ophiolite remnants and juvenile material from island-arc and continental arc sequences (e.g., Heilbron et al., 2017; Klein et al., 2020).

Since missing Paleoproterozoic crustal pieces might be hidden within the basement of younger orogenic belts (e.g., D'Agrella-Filho et al., 2016; Xia and Xu, 2019), their investigation may provide crucial information for Precambrian paleogeographic reconstructions. Within the South American Neoproterozoic orogens, Paleoproterozoic crust is widespread and heterogeneously distributed, being mostly considered as basement inliers or exotic terranes (e.g., Brito Neves et al., 2014). Despite the petrogenetic and geophysical evidence that suggests some degree of correlation with the *neighboring* cratons, the deformational events that developed during the Brasiliano-Pan African orogeny (ca. 0.6–0.5 Ga) strongly recycled the previous stratigraphic record.

Occupying the central portion of West Gondwana, the Borborema Province in NE Brazil, as well its African counterparts, comprise a number of Paleoproterozoic domains bounded by Neoproterozoic belts through regional-scale shear zones (e.g., Santos et al., 2008; Brito Neves et al., 2014; de Caxito et al., 2020). Although the specific nature of the continent-forming mechanisms is poorly understood, the addition of geochronological data has revealed three major periods of crust accretion during the early Paleoproterozoic (i.e., 2.3 Ga, 2.2 Ga and 2.1 Ga; Fetter et al., 2000; Hollanda et al., 2011; Costa et al., 2015; Ferreira et al., 2020) followed by crustal reworking at ca. 2.0–1.9 Ga (Santos et al., 2013a, 2013b; Neves et al., 2015; Santos and Santos, 2019).

In this contribution, we present detailed geochronological (zircon U-Pb and whole-rock Sm-Nd) and geochemical data of metamafic and metaultramafic rocks of the Fazenda Carmo Suite as well as metagranitic and gneissic rocks of the Riacho do Navio Suite. These units occur along the SW termination of the Alto Moxotó Terrane of the Borborema Province and, despite the influence of the Brasiliano-related shear zones, this region preserves old lithosphere, providing a unique opportunity to unravel hidden crustal processes within a Neoproterozoic orogenic belt of West Gondwana.

2. Geological setting

2.1. Regional geology

The Borborema Province constitutes most of the northeastern portion of Brazil (Almeida et al., 1981) and prior to Gondwana breakup, it extended into West Africa through Benin, Nigeria and Cameroon (Fig. 1a; Brito Neves et al., 2000; Van Schmus et al., 2008). Its ancient crustal record is represented by Paleoproterozoic (ca. 2.2–2.0 Ga) gneissic-migmatitic basement inliers as well as local Archean (ca. 3.5–2.6 Ga) nuclei (Brito Neves, 2011; Caxito et al., 2015; Costa et al., 2018). These sequences are overlain or bounded by variably metamorphosed early to late Neoproterozoic (0.9–0.6 Ga) supracrustal fold belts (e.g., Van Schmus et al., 2003; Santos et al., 2019; Caxito et al., 2021) that are intruded by several late Neoproterozoic (ca. 0.6–0.5 Ga) granitic batholiths and stocks that constitute the major tectonic markers of the Brasiliano Orogeny (Santos and Medeiros, 1999; Brito Neves et al., 2016; Sial and Ferreira, 2016; Santos et al., 2020).

In addition to the vast occurrence of granitic batholiths, a prominent feature of the Borborema Province is the dense network of several kilometers-wide shear zones that are interpreted as deep-seated crustal boundaries due to their strong geophysical expression (Oliveira and Medeiros, 2018). Some of them are also considered collisional sutures (Santos et al., 2015a), which fragmented the West Gondwana lithosphere during the late Neoproterozoic (Ganade de Araujo et al., 2014a, 2014b). Among them, the E–W Patos and Pernambuco shear zones divide the province into Northern, Central and Southern subprovinces (Fig. 1b; Van Schmus et al., 1995), and are interpreted either as relics of terrane accretion episodes (Santos et al., 2010; Caxito et al., 2014a, 2014b, Caxito et al., 2016; Padilha et al., 2016), or as intracontinental shallow structures (Neves, 2015).

The Alto Moxotó Terrane is located within the Central Subprovince (Fig. 1c) that also includes the Rio Capibaribe, Alto Pajeú, Piancó Alto-Brigída and São José do Caiano terranes, which are bounded by thrust and strike-slip shear zones (Brito Neves et al., 2000). The Alto Moxotó Terrane is unique in the Central Subprovince because it presents the oldest crustal record, mostly ranging between ca. 2.6 and 2.1 Ga (Santos et al., 2015, Santos et al., 2017b; Brito Neves and Silva Filho, 2020), also including local ca. 1.6 Ga within-plate granites (Lages et al., 2019). The dominance of Paleoproterozoic crust as well as the minor occurrence of Neoproterozoic rocks are contrasting features between this terrane and the adjoining blocks (see Santos et al., 2017a, 2017b for details).

2.2. Local geology

The studied rocks crop out in the SW tail of the Alto Moxotó Terrane in structural contact with the Alto Pajeú Terrane to the north and the Southern Subprovince to the south, via the Serra de Jabitacá and Pernambuco shear zones, respectively (Fig. 2). The oldest unit in the area corresponds to the ca. 2.6 Ga Riacho das Lages Suite that is composed of metagranites and gray gneisses, interpreted as relics of TTG juvenile magmas derived from slab melting (Santos et al., 2017a). In the southern portion of the area, in tectonic contact with the Pernambuco Lineament, lies the E–W elongated Floresta Batholith that comprises a set of ca. 2.1 Ga metagranites, medadiorites and orthogneisses that are interpreted as Cordilleran-like plutonic injections (Santos et al., 2017a). Between these plutonic rocks, there are sillimanite-garnet-biotite paragneisses, schists and fine-grained weathered amphibolites, which are grouped as the Sertânia Complex. This unit is the major supracrustal sequence of the Alto Moxotó Terrane, presenting dominant maximum deposition age around ca. 2.1–1.9 Ga (Santos et al., 2004; Brito Neves and Silva Filho, 2020). Nevertheless, recent detrital zircon dating highlights a late Neoproterozoic contribution suggesting that at least part of the supracrustal succession must be younger (Neves et al., 2017).

The Fazenda Carmo Suite occurs as up to 20 m long × 4–10 m wide elongated lenses in the interior of the Floresta Batholith. They mostly form slightly foliated rocks as the result of the imposed deformation by the E–W Pernambuco Shear Zone. These rocks were originally interpreted as intrusive into this Batholith (Santos, 1995), but due to their limited exposure, we were not able to clearly verify the intrusive contact. They crop out as metric boulders or concordant lenses along regional foliation planes, being mostly composed of medium- to fine-grained metamafic members such as slightly foliated amphibolite blocks (Fig. 3a) that might exhibit facies with well-developed centimetric garnet neoblasts (Fig. 3b) or massive metagabbros (Fig. 3c). Minor coarse-grained ultramafites are present, being mostly represented by garnet-free metapyroxenites that might be partially retrogressed to chlorite-bearing amphibolites (Fig. 3d).

Amphibolites are characterized by poorly developed nematoblastic texture (Fig. 3e), presenting subhedral hornblende (60%) and euhedral to subhedral plagioclase (30%) with variable degrees

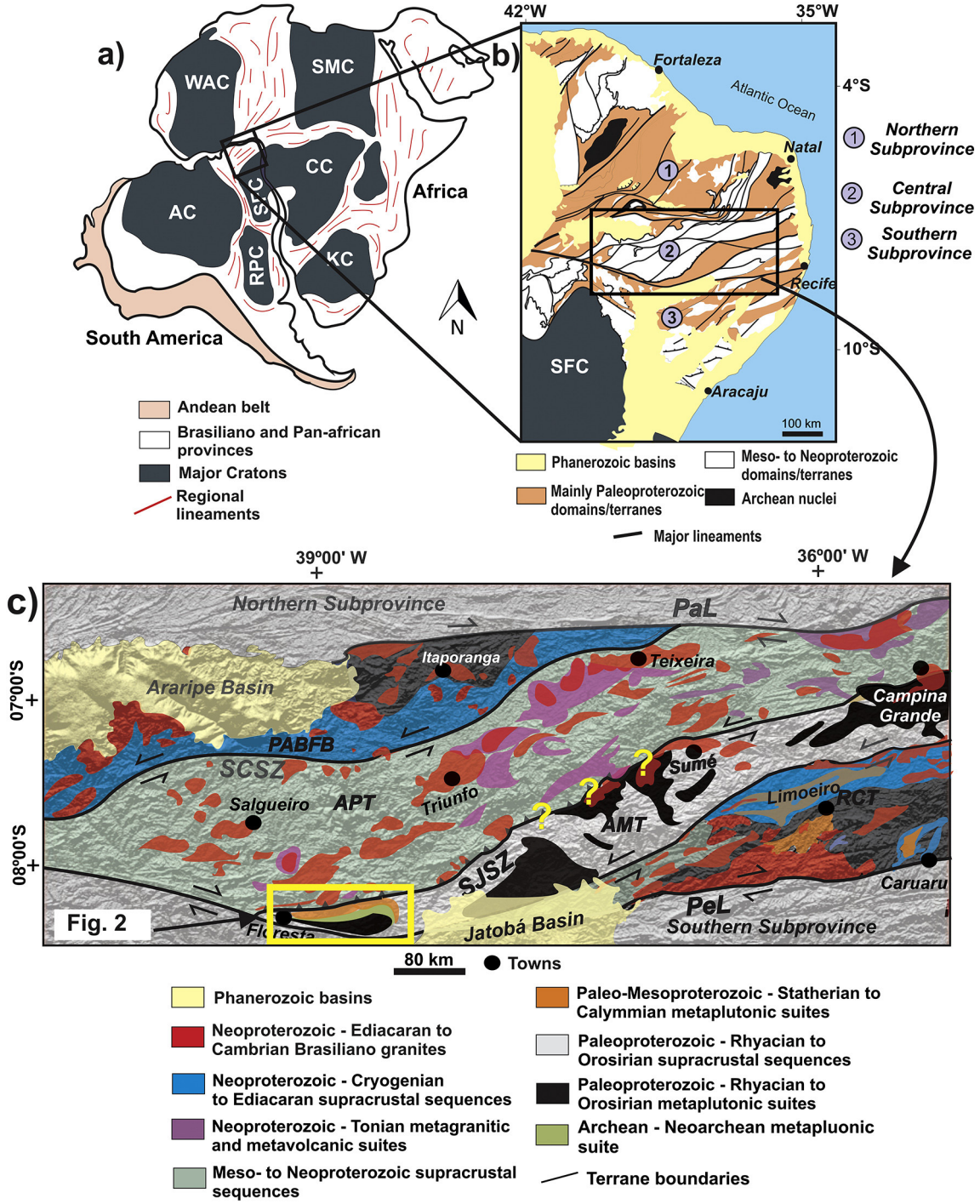

Fig. 1. (a) Geodynamic context of the Borborema Province on a paleogeographic reconstruction of West Africa and Northeast South America; (b) Simplified tectonic sketch of the Borborema Province; (c) Geological map of part of the Central Subprovince with the studied area highlighted by the yellow rectangle.

of saussuritization, including neoformed tiny zoisite and chlorite crystals. Minor euhedral diopside (5%) represents an early magmatic phase, whereas zircon and apatite correspond to less than 2% of the rock mineralogy. Subhedral granular ilmenite represents the main opaque oxide mineral. The most foliated members exhibit elongated amphibole crystals deformed along the foliation planes (Fig. 3f), whereas garnet-bearing facies exhibit similar mineralogy, but contains 0.5 cm euhedral and strongly fractured pink garnet porphyroblasts that exhibit poikiloblastic texture with tiny rutile and plagioclase inclusions.

The metagabbros are composed of subhedral pale green diopside (50%), subhedral to anhedral dark green augite (10%) and subhedral dark gray plagioclase (40%). The latter is characterized by low- to moderate degrees of sericitization. Uralitization processes are marked by neophormed euhedral hornblende crystals that are present but not common, whereas zircon crystals occur as tiny inclusions in dark brown intercrystalline biotite films. Zircon, apatite, and ilmenite occur in the same proportions of the amphibolites. The metapyroxenites are composed of pale gray euhedral to subhedral diopside (30%–55%) and bronzite (5%–25%) crystals,

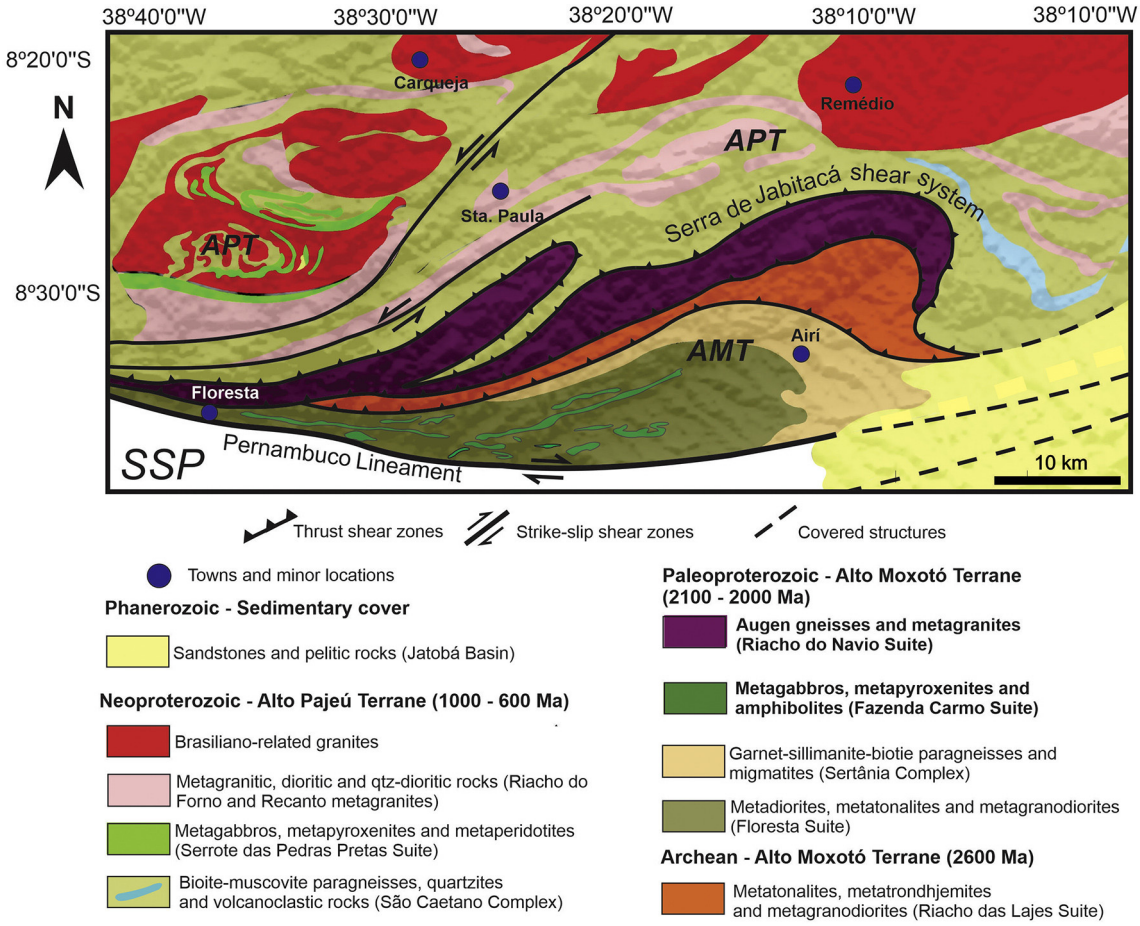

Fig. 2. Geological map of the studied area. APT–Alto Pajeú Terrane, AMT–Alto Moxotó Terrane, SSP–Southern Subprovince.

whereas the surrounding groundmass is formed of aggregates of subhedral hornblende (15%–25%) and anhedral plagioclase (5%). They are classified as metaclinopyroxenites or metawebsterites, depending on the orthopyroxene proportion and as in the metamafic members, deformation and recrystallization obliterated the magmatic fabric. Also, tiny chorite-epidote venules crosscut these rocks filling local microfractures.

In contrast, the Riacho do Navio Suite is characterized by leuco- to mesocratic metagranites and orthogneisses that crop out along gentle dipping foliation planes related to the Serra de Jabitacá Shear Zone (Fig. 3g). These rocks exhibit variable degrees of deformation, including slightly deformed porphyritic members to highly deformed augen-gneisses (Fig. 3h). Relics of muscovite-bearing rocks described in the Alto Pajeú Terrane also occur interleaved with these rocks, being interpreted as tectonic slices that were thrust toward the Alto Moxotó Terrane (Santos et al., 2017b). The metagranite members are medium- to coarse-grained and exhibit weak foliation characterized by tiny phyllosilicate alignments. They are composed by euhedral to subhedral quartz (35%), subhedral plagioclase phenocrysts (30%), subhedral orthoclase and microcline (25%), muscovite (4%) and biotite (4%). Millimetric euhedral garnet porphyroblasts occur in some samples and along with zircon, apatite, and ilmenite, correspond to less than 3% of the rock mineralogy. The augen-gneiss samples present very similar mineralogy except for punctual euhedral to anhedral monazite grains. Due to the high recrystallization degree, quartz ribbons with well-developed undulose extinction and sigmoidal plagioclase and orthoclase are typical in the gneissic members (Fig. 3i).

3. Analytical methods

Representative fresh rock samples of the studied suites were selected for isotopic U-Pb and whole-rock Sm-Nd measurements as well as whole-rock geochemistry. Zircon crystals were extracted from four samples, two of each unit for U-Pb dating at the Geochronology Laboratory of the Universidade de Brasília, Brazil and the results are listed in Tables 1–4. Standard techniques, including sample crushing and sieving were performed, followed by heavy mineral separation through gravimetric and magnetic methods. The remaining zircon grains were handpicked using a binocular microscope and mounted in epoxy resins for Laser Ablation Inductively Coupled Plasma Mass Spectrometry (LA-ICP-MS) isotope ratio acquisition. Cathodoluminescence and back-scattered images were used to investigate the internal structure of each zircon crystal prior the isotopic analysis.

A Thermo Finnigan Neptune Multi Collector ICPMS equipped with a secondary electron multiplier-ion counter was used for U-Pb data acquisition. Only coherent interval analyses were chosen to avoid signal mixed ages. Normalization was performed with the GJ-1 primary standard zircon ($^{207}Pb/^{206}Pb$ age = 608.3 Ma, $^{206}Pb/^{238}U$ age = 600.7 Ma and $^{207}Pb/^{235}U$ age = 602.2 Ma; Jackson et al., 2004), whereas the 91500 zircon standard (ID-TIMS 1065.4 ± 0.3 Ma; Wiedenbeck et al., 2004) was analyzed as a secondary reference material and the obtained ages are 1042 ± 27 Ma ($^{207}Pb/^{206}Pb$ age), 1055 ± 14 Ma ($^{207}Pb/^{235}U$ age) and 1064 ± 10 Ma ($^{206}Pb/^{238}U$ age). Data reduction followed Bühn et al. (2009) and Matteini et al. (2010) and the obtained ages

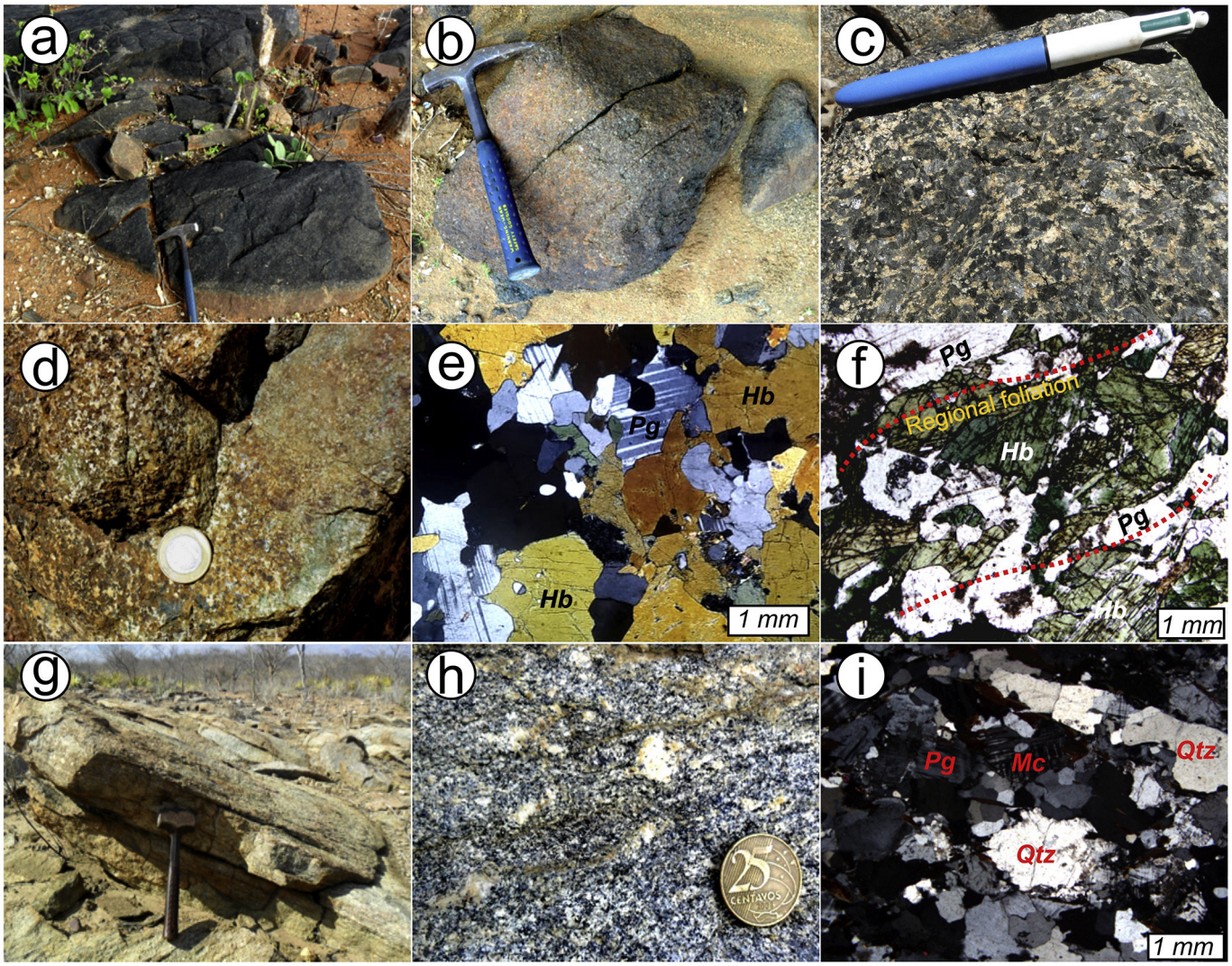

Fig. 3. Field aspects of the studied units. Fazenda Carmo Suite: (a) slightly foliated bounder of amphibolite; (b) block of garnet-bearing amphibolite; (c) coarse-grained metagabbro; (d) metapyroxenite boulder exhibiting green-colored alteration minerals; (e) granoblastic texture on less deformed amphibolite; (f) amphibolite exhibiting elongated hornblende crystals along foliation planes imposed by the regional deformation. Riacho do Navio Suite: (g) gentle-dipping sheet of metagranitic rock due to thrust tectonics; (h) augen-gneiss facies exhibiting deformed K-feldspar porphyroclast; (i) recrystallized fabric of orthogneiss exhibiting intense quartz recrystallization, including ribbon-like crystals. Hb–hornblende, Pg–plagioclase, Mc–microcline, Qtz–quartz.

Table 1
Summary of LA-ICP-MS data of zircons from sample GL-01B (correlated with the Fazenda Carmo Suite).

Grain spot	Isotope ratios						Age (Ma)								
	$^{207}Pb/^{206}Pb$	±1σ	$^{207}Pb/^{235}U$	±1σ	$^{206}Pb/^{238}U$	±1σ	$^{207}Pb/^{206}Pb$	±2σ	$^{207}Pb/^{235}U$	±2σ	$^{206}Pb/^{238}U$	±2σ	Rho	Th/U	Disc. (%)
04-ZR2	0.12863	1.14	6.340	1.60	0.3574	1.06	2079	40	2024	28	1970	36	0.66	0.231	5.26
03-ZR1	0.12951	1.65	6.611	2.37	0.3702	1.66	2091	57	2061	41	2030	58	0.70	0.225	2.92
06-ZR4	0.12538	1.52	5.846	2.37	0.3381	1.77	2034	53	1953	41	1878	58	0.75	0.169	7.70
05-ZR3	0.13020	1.78	5.601	2.88	0.3120	2.24	2101	62	1916	49	1750	69	0.78	0.243	16.68
16-ZR11	0.12180	2.16	5.489	2.92	0.3268	1.93	1983	76	1899	50	1823	61	0.66	0.139	8.05
38-ZR27	0.12721	2.31	5.685	2.95	0.3241	1.80	2060	80	1929	50	1810	57	0.61	0.258	12.14
10-ZR8	0.12833	2.49	6.222	3.31	0.3516	2.15	2075	87	2008	57	1942	72	0.65	0.258	6.40
07-ZR5	0.12124	2.02	4.556	2.57	0.2725	1.55	1974	71	1741	42	1554	43	0.60	0.186	21.32
09-ZR7	0.11215	1.96	3.798	2.72	0.2456	1.86	1835	70	1592	43	1416	47	0.68	0.250	22.83

were calculated using Isoplot version 4.1 (Ludwig, 2012), avoiding spots with high common Pb concentrations.

Nineteen samples were selected for Sm-Nd measurements that were also conducted at the Geochronology Lab of the Universidade de Brasília and the results are presented in Table 5. Part of the presented Sm-Nd results were already published by Santos et al. (2018) but in a paper with a different focus. For these analyses, the method described in Gioia and Pimentel (2000) was followed. Whole rock powders (~50 mg) were mixed with a ^{149}Sm-^{150}Nd spike solution and dissolved in Savillex capsules. The extraction of Sm and Nd from whole rock samples followed conventional cation exchange techniques using Teflon columns containing LN-

Table 2
Summary of LA-ICP-MS data of zircons from sample MV-03 (Fazenda Carmo Suite).

Grain spot	Isotope ratios						Age (Ma)								
	$^{207}Pb/^{206}Pb$	±1σ	$^{207}Pb/^{235}U$	±1σ	$^{206}Pb/^{238}U$	±1σ	$^{207}Pb/^{206}Pb$	±2σ	$^{207}Pb/^{235}U$	±2σ	$^{206}Pb/^{238}U$	±2σ	Rho	Th/U	Disc. (%)
016-Z8	0.113	0.44	3.849	0.84	0.247	0.71	1796	8	1603	7	1423	9	0.82	0.388	20.74
020-Z12	0.113	0.41	3.933	0.76	0.252	0.64	1800	8	1621	6	1449	8	0.80	0.071	19.49
025-Z14	0.131	0.39	6.677	0.71	0.371	0.59	2057	7	2070	6	2032	10	0.78	0.244	1.22
027-Z16	0.132	0.33	7.076	1.08	0.389	1.02	2072	6	2121	10	2120	19	0.94	0.494	2.35
028-Z17	0.128	0.69	6.144	1.03	0.348	0.76	2019	13	1997	9	1927	13	0.71	0.365	4.51
030-Z19N	0.131	0.31	6.754	0.80	0.373	0.74	2066	6	2080	7	2043	13	0.90	0.245	1.07
040-Z26	0.129	0.37	6.242	1.02	0.350	0.95	2036	7	2010	9	1937	16	0.92	0.195	4.89
045-Z28B	0.129	0.43	6.194	0.79	0.348	0.66	2036	8	2004	7	1924	11	0.80	0.295	5.51
049-Z30B	0.110	0.41	3.639	0.79	0.239	0.68	1753	8	1558	6	1383	8	0.82	0.174	21.12

Table 3
Summary of LA-ICP-MS data of zircons from sample MV-11 (Fazenda Carmo Suite).

Grain spot	Isotope ratio						Age (Ma)								
	$^{207}Pb/^{206}Pb$	±1σ	$^{207}Pb/^{235}U$	±1σ	$^{206}Pb/^{238}U$	±1σ	$^{207}Pb/^{206}Pb$	±1σ	$^{207}Pb/^{235}U$	±1σ	$^{206}Pb/^{238}U$	±2σ	Rho	Th/U	Disc. (%)
011-Z07	0.060	1.01	0.820	6.90	0.099	6.43	616	21	611	7	609	6	0.72	0.01	1.13
018-Z12	0.127	0.59	3.322	7.66	0.219	8.68	1803	10	1486	7	1275	9	0.85	0.08	29.31
021-Z13	0.126	0.45	5.842	9.00	0.336	15.1	2046	8	1953	9	1867	15	0.88	0.07	8.72
023-Z15	0.127	0.42	5.735	9.48	0.328	16.0	2058	7	1939	9	1830	16	0.91	0.19	11.0
024-Z16	0.123	0.56	5.675	9.45	0.333	15.1	2009	10	1928	9	1854	15	0.92	0.53	7.75
030-Z20	0.127	0.67	6.085	7.96	0.346	10.2	2064	12	1989	8	1917	10	0.78	0.28	7.09
033-Z21	0.124	0.39	5.536	10.84	0.322	18.8	2028	7	1907	11	1797	19	0.94	0.10	11.38
035-Z23	0.058	0.47	0.790	3.77	0.099	4.00	550	10	595	4	607	4	0.79	0.15	10.44
036-Z24	0.122	0.50	5.498	6.78	0.325	9.59	1995	9	1901	7	1816	10	0.80	0.34	8.98
042-Z28	0.116	1.46	4.069	19.48	0.256	1.88	1902	26	1658	19	1472	25	0.92	0.09	22.6

Table 4
Summary of LA-ICP-MS data of zircons from sample FL-119 (Riacho do Navio Suite).

Grain spot	Isotope ratio						Age (Ma)								
	$^{207}Pb/^{206}Pb$	±1σ	$^{207}Pb/^{235}U$	±1σ	$^{206}Pb/^{238}U$	±1σ	$^{207}Pb/^{206}Pb$	±2σ	$^{207}Pb/^{235}U$	±2σ	$^{206}Pb/^{238}U$	±2σ	Rho	Th/U	Disc. (%)
050-ZR25N	0.114	0.61	3.972	1.04	0.252	0.75	1869	22	1628	17	1449	19	0.72	0.710	22.51
015-ZR6	0.066	0.74	0.963	1.86	0.104	1.67	835	31	685	18	640	20	0.89	3.755	23.32
024-ZR9B	0.073	0.92	1.135	1.45	0.112	1.06	1015	37	770	16	688	14	0.73	0.223	32.16
014-ZR5	0.127	0.66	6.931	1.42	0.394	1.20	2061	23	2103	25	2145	44	0.85	0.750	4.08
046-ZR21B	0.059	1.20	0.781	1.77	0.095	1.24	587	52	586	16	586	14	0.70	0.036	0.20
034-ZR14	0.122	0.65	5.461	1.49	0.322	1.29	1999	23	1894	25	1801	40	0.86	0.615	9.89
043-ZR19	0.106	0.54	2.932	1.23	0.199	1.04	1743	20	1390	19	1172	22	0.85	0.096	32.78
056-ZR28	0.098	1.01	2.244	1.84	0.165	1.50	1588	37	1195	26	990	27	0.81	0.234	37.68
055-ZR27	0.125	0.46	6.022	0.93	0.349	0.72	2031	16	1979	16	1930	24	0.77	0.968	4.98
010-ZR4N	0.111	0.78	3.424	1.74	0.222	1.51	1823	28	1510	27	1297	35	0.87	0.829	28.84
009-ZR3B	0.097	0.54	2.176	1.33	0.162	1.16	1571	20	1173	18	970	21	0.87	0.174	38.28
027-ZR11	0.120	0.47	4.794	1.47	0.288	1.34	1962	17	1784	25	1635	39	0.91	1.146	16.65
044-ZR20	0.124	0.48	5.835	1.08	0.338	0.90	2027	17	1952	19	1881	29	0.83	1.396	7.18
058-ZR30N	0.125	0.56	5.950	0.95	0.344	0.67	2033	20	1969	16	1907	22	0.71	1.059	6.19
008-ZR3N2	0.106	0.40	2.856	1.00	0.194	0.84	1742	15	1371	15	1145	18	0.84	0.125	34.27
023-ZR9N	0.118	0.48	4.400	1.37	0.268	1.23	1939	17	1712	23	1533	33	0.90	1.242	20.92
035-ZR15N	0.131	0.98	7.871	1.63	0.434	1.25	2115	34	2216	29	2328	49	0.77	0.594	10.05
057-ZR29	0.124	0.58	5.497	1.33	0.320	1.14	2019	21	1900	23	1793	36	0.85	1.149	11.19
045-ZR21N	0.119	0.41	4.382	1.04	0.266	0.88	1946	14	1709	17	1522	24	0.85	0.370	21.79
048-ZR23	0.120	0.52	4.621	1.96	0.277	1.85	1970	19	1753	32	1577	52	0.95	0.749	19.95
047-ZR22	0.114	0.48	3.569	1.14	0.226	0.96	1873	17	1543	18	1313	23	0.85	0.901	29.86
025-ZR10N	0.083	0.66	1.414	1.00	0.123	0.66	1272	26	895	12	750	9	0.66	0.467	41.06
007-ZR3N	0.117	0.38	4.024	1.62	0.247	1.53	1925	13	1639	26	1425	39	0.95	0.638	25.98
004-ZR1N	0.112	0.60	3.313	2.90	0.213	2.81	1841	22	1484	45	1247	64	0.97	0.822	32.25
013-ZR4B	0.080	1.09	1.308	1.38	0.117	0.76	1212	43	849	16	717	10	0.55	0.325	40.79
054-ZR26	0.126	0.56	5.536	1.19	0.317	0.98	2048	20	1906	20	1779	30	0.82	0.988	13.12
029-ZR13N	0.121	0.71	4.501	2.03	0.268	1.87	1978	25	1731	34	1535	51	0.92	0.853	22.40
005-ZR1B	0.07917	1.54	1.257	2.02	0.1151	1.26	1176	60	826	23	702	17	0.62	0.332	40.30
039-ZR18N	0.13045	0.78	6.620	1.67	0.3680	1.43	2104	27	2062	29	2020	49	0.86	0.611	22.51

Spec resin (HDEHP – diethylhexyl phosphoric acid supported on PTFE powder). The Sm and Nd samples were loaded on Re evaporation double-filament assemblies and the isotopic measurements were performed using a Triton Plus Thermoscientific multicollector mass spectrometer in the static mode.

The uncertainties in the $^{147}Sm/^{143}Nd$ and $^{143}Nd/^{144}Nd$ ratios were better than ±0.2% (2σ) and ±0.0064% (1σ), respectively, based on repeated analyses using the BHVO-2 international rock standard. The $^{143}Nd/^{144}Nd$ ratios were normalized to a $^{146}Nd/^{144}Nd$ ratio of 0.7219 and a decay constant of 6.54×10^{-12} y^{-1} was used

Table 5
Summary of Nd isotope data for the Fazenda Carmo (F.C.S.) and Riacho do Navio (R.N.S.) suites. Crystallization ages used are 2.12 Ga and 2.08 Ga.

Sample	Unit	Sm (ppm)	Nd (ppm)	$^{147}Sm/^{144}Nd$	$^{143}Nd/^{144}Nd$ (±2SE)	$\varepsilon_{Nd}(0)$	$\varepsilon_{Nd}(t)$	T_{DM} (Ga)
GL01B	F.C.S.	0.54	2.25	0.145	0.511930 (±12)	−13.80	+0.27	2.46
GL01C	F.C.S.	3.65	13.54	0.1632	0.512230 (±07)	−7.97	+1.17	2.45
GL02B	F.C.S.	3.02	12.45	0.1468	0.512049 (±12)	−11.49	+2.11	2.25
FL63	F.C.S.	1.99	9.86	0.1223	0.511955 (±11)	−13.32	+0.59	2.43
MV3	F.C.S.	0.45	1.94	0.1123	0.511458 (±61)	−23.02	−0.03	3.34
FL124	R.N.S.	4.47	24.08	0.0749	0.511571 (±11)	−20.81	+1.70	2.2
FL100	R.N.S.	3.44	21.24	0.0978	0.511233 (±14)	−27.41	−1.04	2.37
FL117	R.N.S.	2.51	12.89	0.1175	0.511533 (±06)	−21.56	−0.44	2.38
FL25	R.N.S.	4.46	26.57	0.1015	0.511279 (±15)	−26.51	−1.13	2.39
FL101	R.N.S.	6.18	35.17	0.1063	0.511341 (±12)	−25.30	−1.20	2.41
FL51A	R.N.S.	10.34	60.90	0.1026	0.511253 (±13)	−27.02	−1.94	2.45
FL99	R.N.S.	4.54	25.97	0.1059	0.511325 (±10)	−25.61	−1.41	2.42
FL125	R.N.S.	10.84	54.52	0.1202	0.511484 (±05)	−22.51	−2.12	2.54
FL95A	R.N.S.	6.61	36.76	0.1088	0.511277 (±17)	−26.55	−3.13	2.56
FL120A	R.N.S.	4.51	30.41	0.0896	0.510933 (±13)	−33.26	−4.73	2.58
FL123	R.N.S.	2.47	29.21	0.0719	0.510579 (±13)	−40.16	−6.92	2.64
FL119	R.N.S.	4.30	24.59	0.1034	0.510985 (±13)	−32.24	−7.41	2.84
FL122	R.N.S.	5.60	35.15	0.0964	0.510797 (±07)	−35.91	−9.22	2.92

(Lugmair and Marti, 1978), whereas the T_{DM} model ages were calculated using the DePaolo (1981) model.

Nineteen fresh samples were carefully selected for whole-rock geochemical analyses and the results are presented in Tables 6 and 7. Samples from the Fazenda Carmo Suite were analyzed at the Geosol laboratory in Brazil, whereas those from the Riacho do Navio Suite were analyzed at the ALS (Peru) laboratory, following similar methodologies. Major and trace elements were analyzed via inductively coupled plasma atomic emission spectroscopy (ICP-AES) with detection limit of 0.01%. ICP-MS with detection limit between 0.01 and 0.5 ppm after fusion using Li meta- and tetraborate as well as digestion with nitric acid. The difference in sample weight before and after heating at 1000 °C for 1 h was used to determine the percentage of loss on ignition. The presented geochemical diagrams were generated by Igpet 6, GCDKIT and Petrograph softwares as well as in-house developed Excel spreadsheets.

4. Results

4.1. U-Pb geochronology

Sample GL01B is a coarse-grained hornblendite with interstitial plagioclase (up to 15%) obtained close to Floresta Town (4 km to ESE; geographic coordinates 38°32′18″W and 08°36′20″S) and exposed as large lenses within the Floresta Batholith. A total of twenty-three zircon crystals were analyzed, but most presented high degrees of metamictization and only nine grains were used for age calculation. They are pale gray presenting axial ratios of 1:2 and subrounded shapes with sizes less than 100 μm (Fig. 4a). They are euhedric to subhedric, present poorly developed oscillatory zoning and Th/U ratios ranging from 0.14 to 0.26, which are typical features of magmatic crystals. The concordia diagram (Fig. 5a) yielded an upper intercept age of 2119 ± 42 Ma (n = 9) with MSWD = 0.8, interpreted as the crystallization age of the protolith.

Sample MV03 is a slightly foliated garnet metagabbro collected around 37 km away from Floresta Town (geographic coordinates 38°15′20″W and 08°36′17″S) at a concordant contact with the regional foliation. Extracted zircon crystals are pale gray, present axial ratios from 1:2 to 1:3 and are subhedral (rounded) to anhedral with sizes ranging from 50 to 100 μm (Fig. 4b). They are randomly fractured, present poorly developed oscillatory zoning and core and rim structures as well, typical of overgrowth events.

Table 6
Major (wt.%) and trace element (ppm) concentrations of samples from the Fazenda Carmo Suite.

	Major elements (wt.%)						
	GL-001C	GL-002B	GL-003B	RS-013	MV-03	LS-93A	GL-001C.2
SiO_2	42.6	44.7	52.4	48.8	44.3	44.7	49.7
TiO_2	1.34	0.91	1.8	2.2	1.28	3.11	0.97
Al_2O_3	18.2	18.2	14.1	12.8	17.3	14.6	18.3
$Fe_2O_3^t$	16.3	13.4	15.3	17.9	15.9	16.8	12.4
MnO	0.23	0.2	0.22	0.24	0.24	0.22	0.17
MgO	7.05	7.89	5.33	5.73	6.49	6.09	5.78
CaO	12.1	13.2	8.35	9.77	11.1	9.77	8.81
Na_2O	1.62	1.14	2.38	1.93	1.67	2.46	2.49
K_2O	0.26	0.22	0.43	0.55	0.23	0.56	0.53
P_2O_5	0.196	0.169	0.217	0.174	0.19	0.34	0.42
LOI	1.22	0.89	0.36	0.48	1.29	1.25	0.44
Total	101.1	100.9	100.9	100.6	100.2	99.9	100.1
	Trace and rare earths elements-REE (ppm)						
Co	42	47.1	52.5	79	37.5		[a]
Ni	4.3	17.2	37.7	51	16	[a]	[a]
Cu	76.2	5	41.7	287.5	96	[a]	[a]
Tl	[a]	[a]	0.02	0.05	[a]	[a]	[a]
Rb	0.2	0.12	0.2	3.8	1.7	[a]	1.5
Sn	0.8	0.8	1.2	0.9	[a]	[a]	[a]
Sr	404.5	353	359.2	137.2	411	361.2	292.5
W	0.1	[a]	[a]	[a]	2.4	[a]	[a]
Zr	24.1	26	26.2	24.2	26	26.2	26.4
Cs	[a]	[a]	[a]	[a]	0.08	0.2	0.8
Ba	107	97	129	128	71	[a]	[a]
La	27.2	6.9	12.4	15.1	5.2	18.5	22.3
Ce	15	12.7	15.4	25.8	12.3	20.5	24.9
Pr	6.66	2.7	3.79	4.29	2.22	5.15	9.99
Nd	26.3	12.6	17.1	18.7	10.9	23.6	21.7
Sm	5.6	3.4	4.3	4.6	2.9	5.18	7.73
Eu	1.7	1.07	1.37	1.56	1.06	1.86	2.2
Gd	4.89	3.58	4.23	5.14	3.32	5.19	6.18
Tb	0.67	0.51	0.7	0.79	0.5	0.77	0.92
Dy	3.82	2.98	4.31	4.95	3.1	4.1	4.68
Ho	0.72	0.63	0.89	1	0.67	0.76	0.91
Er	1.9	1.74	2.46	2.73	1.88	2.41	2.57
Tm	0.27	0.23	0.35	0.4	0.24	0.31	0.36
Yb	1.6	1.5	2.3	2.5	1.6	1.2	[a]
Lu	0.21	0.18	0.29	0.34	0.2	0.29	0.35
Y	1.5	1.5	2.3	2.5	1.6	1.5	1.6
Hf	0.71	0.72	0.92	0.97	0.19	[a]	[a]
Th	5.2	3.8	3.8	[a]	3.9	3.8	[a]
U	1.04	1.56	0.38	[a]	[a]	[a]	[a]
Mg[a]	32.46	39.55	27.91	26.24	31.11	28.70	34.10

[a] Below detection limit. Total iron reported as $Fe_2O_3^t$.

Table 7
Major (wt.%) and trace element (ppm) concentrations of samples from the Riacho do Navio Suite.

	Major elements (wt.%)											
	RN1	RN2	RN3	RN4	RN5	RN6	RN7	FL99	FL100	FL102	FL103	FL104
SiO_2	70.1	72.1	70.2	69.5	69.5	75	73.4	74.2	74.1	73.5	74.4	75.9
TiO_2	0.75	0.8	0.74	0.76	0.75	0.3	0.31	0.13	0.13	0.11	0.27	0.26
Al_2O_3	12.7	11.8	13.6	12.9	16.5	13.4	14.4	16.8	16.8	14.2	13.4	13.2
$Fe_2O_3^t$	2.76	4.59	5	4.37	4.16	2.83	2.57	1.08	1.06	1.97	2.01	1.97
Cr_2O_3	0.01	0.01	0.01	0.01	0.01	0.02	0.01	0.01	0.01	0.01	0.01	0.01
MnO	0.06	0.05	0.05	0.04	0.04	0.04	0.03	0.02	0.02	0.02	0.03	0.03
MgO	1.02	1.08	1.22	0.96	0.93	0.48	0.65	0.14	0.14	0.12	0.4	0.4
CaO	2.12	2.04	1.9	1.84	1.98	1.34	1.15	0.84	0.84	0.75	1.34	1.31
Na_2O	3.75	3.41	3.1	3.25	3.28	3.28	3.25	3	3	3.92	3.37	3.31
K_2O	5.83	4.03	4.74	5.2	4.69	4.22	5.29	4.79	4.85	4.85	4.27	4.15
P_2O_5	0.28	0.28	0.24	0.21	0.23	0.12	0.13	0.05	0.04	0.05	0.09	0.08
LOI	1.00	0.29	0.05	1.80	0.05	0.20	0.15	0.05	0.07	1.00	0.70	0.55
Total	100.3	100.4	100.8	100.8	102.1	101.2	101.3	101.1	101.1	100.5	100.2	101.1
	Trace and rare earths elements-REE (ppm)											
V	49	54	47	44	43	20	22	17	17	21	14	15
Cr	60	80	70	60	70	100	60	10	10	20	10	10
Ga	26.1	27.8	26.7	27.4	27.6	21.3	21.1	19.4	19.8	18.3	22.1	22.3
Rb	221	128	218	223	218	206	236	186	183	155.5	194.5	202
Sn	3	4	4	4	4	4	3	2	2	1	4	3
Sr	270	255	229	264	265	142.5	160	85.6	84	74.4	138.5	140
W	5	4	3	3	4	6	3	510	547	642	422	430
Zr	763	703	600	584	741	242	242	143	98	138	243	230
Nb	29.4	37.1	26.4	26.7	27.8	15	14	6.7	6.7	5.7	13.3	13.6
Cs	1.62	1.44	1.7	1.61	1.56	1.21	1.21	0.94	0.93	0.79	1.03	0.97
Ba	1400	915	1195	1450	1330	513	781	349	340	286	520	508
Pb	25	17	24	26	24	33	37	[a]	[a]	[a]	[a]	[a]
La	258	150.5	173.5	252	279	93.5	100.5	40.5	39.1	40	86.6	86.6
Ce	417	318	346	427	424	173.5	179.5	79.1	75.2	70.9	151	150.5
Pr	43	25.3	29.5	42.7	47.3	15.8	15.85	7.22	6.84	6.74	14.15	13.75
Nd	132	78.5	90.4	129	145.5	48.6	49.1	23.2	21.8	22.6	46.4	44.7
Sm	15.75	11.05	11.9	17.15	18.55	7.69	6.94	4.18	4	3.92	6.81	7
Eu	2.14	1.6	1.48	2.19	2.25	0.87	0.9	0.52	0.54	0.53	0.91	0.81
Gd	10.1	7.23	7.22	9.61	9.77	5.19	4.23	3.4	3.17	3.12	4.66	4.4
Tb	1.24	0.92	0.85	1.03	1.24	0.69	0.54	0.55	0.46	0.49	0.69	0.64
Dy	5.9	4.76	4.07	4.89	5.19	3.91	3.22	2.91	2.84	2.96	3.84	3.45
Ho	0.9	0.81	0.69	0.76	0.81	0.64	0.55	0.59	0.54	0.56	0.6	0.57
Er	2.02	1.86	1.75	1.49	2.03	1.57	1.35	1.67	1.54	1.63	1.61	1.44
Tm	0.33	0.29	0.21	0.22	0.25	0.2	0.2	0.27	0.23	0.22	0.19	0.19
Yb	1.71	1.06	1.29	1.2	1.4	0.96	1.26	1.53	1.3	1.5	1.26	1.03
Lu	0.19	0.15	0.16	0.13	0.17	0.14	0.16	0.21	0.18	0.21	0.16	0.14
Y	26.1	21.7	19.7	20.3	22.1	17	16.7	17.8	16.2	17.2	17.8	17.4
Hf	18.3	16.6	13.6	12.9	18.4	6.2	5.9	4.4	3.3	4.8	7.6	7
Ta	2.6	2.4	2.7	2.5	2.5	1.1	0.9	0.6	0.6	0.6	0.9	0.9
Th	85.9	84.8	73.4	72.6	77.9	66.3	50.9	30.8	31.5	29.4	64.7	60.8
U	2.02	1.52	1.67	1.47	1.55	3.57	4.13	8.16	8.19	6.55	3.82	3.62

[a] Below detection limit. Total iron reported as $Fe_2O_3^t$.

Analyzed spots were mostly focused on the inner portions of the grains and the obtained Th/U ratios range from 0.17 to 0.40, which are typical from an igneous origin. Zircon crystal 020-Z12 presented the lowest Th/U ratio (0.07), which might be related to a metamorphic overprint or mixed processes. On the concordia diagram (Fig. 5b), a cluster of 09 spots yield an upper intercept age of 2130 ± 30 Ma, interpreted as the crystallization age of the protolith, whereas the lower intercept marks an age of 802 ± 31 Ma, being related to Pb loss during metamorphism (MSWD = 0.8). In addition, five zircon crystals were also extracted from this sample but did not present acceptable response due to their high common Pb concentrations.

Sample MV11 is a metawebsterite collected from a 1 m-long 30 cm thick layer within metagabbros located just 1 km from where sample MV03 was collected. It corresponds to one of the few preserved and relatively fresh ultramafites collected from the Fazenda Carmo Suite. As expected for primitive rocks, the sample is zircon-poor, but after almost 70 kg of sample crushing, a cluster of fourteen zircon grains were recovered, but only nine presented minimally acceptable results. These crystals range from 70 to 190 μm along their major axes, being mostly subhedral and lacks clear oscillatory zoning (Fig. 4c). Most crystals present high Th/U ratios that range between 0.14 and 0.53, but lower ratios (<0.1) were observed on Z07 ($^{207}Pb/^{235}U$ age = 611 Ma), Z08 ($^{207}Pb/^{235}U$ age = 1486 Ma) and Z28 ($^{207}Pb/^{235}U$ age = 1658 Ma) ($^{207}Pb/^{235}U$ age = 611 Ma) grains, suggesting Pb loss episodes that might be interpreted as heating events during the Brasiliano Orogeny. Along the obtained discordia line (Fig. 5c), the sample yields an upper intercept age of 2085 ± 22 Ma, whereas the 619 ± 50 Ma age marks the lower intercept (MSWD = 4.8), interpreted as the best estimations for the protolith crystallization age and the Brasiliano metamorphic overprint, respectively.

Sample FL119 corresponds to a metamonzogranite collected in the inner portion of the Riacho do Navio Suite (geographic coordinates 38°02′24″W and 08°28′29″S) to minimize the influence of the regional deformation. The collected zircon crystals are colorless to slightly yellow with axial ratios ranging from 1:1 to 1:4. They range in size from 80 to 120 μm, are subhedral to euhedral and might present symmetric oscillatory zoning, which is indicative of a magmatic origin. However, recrystallization rims are always

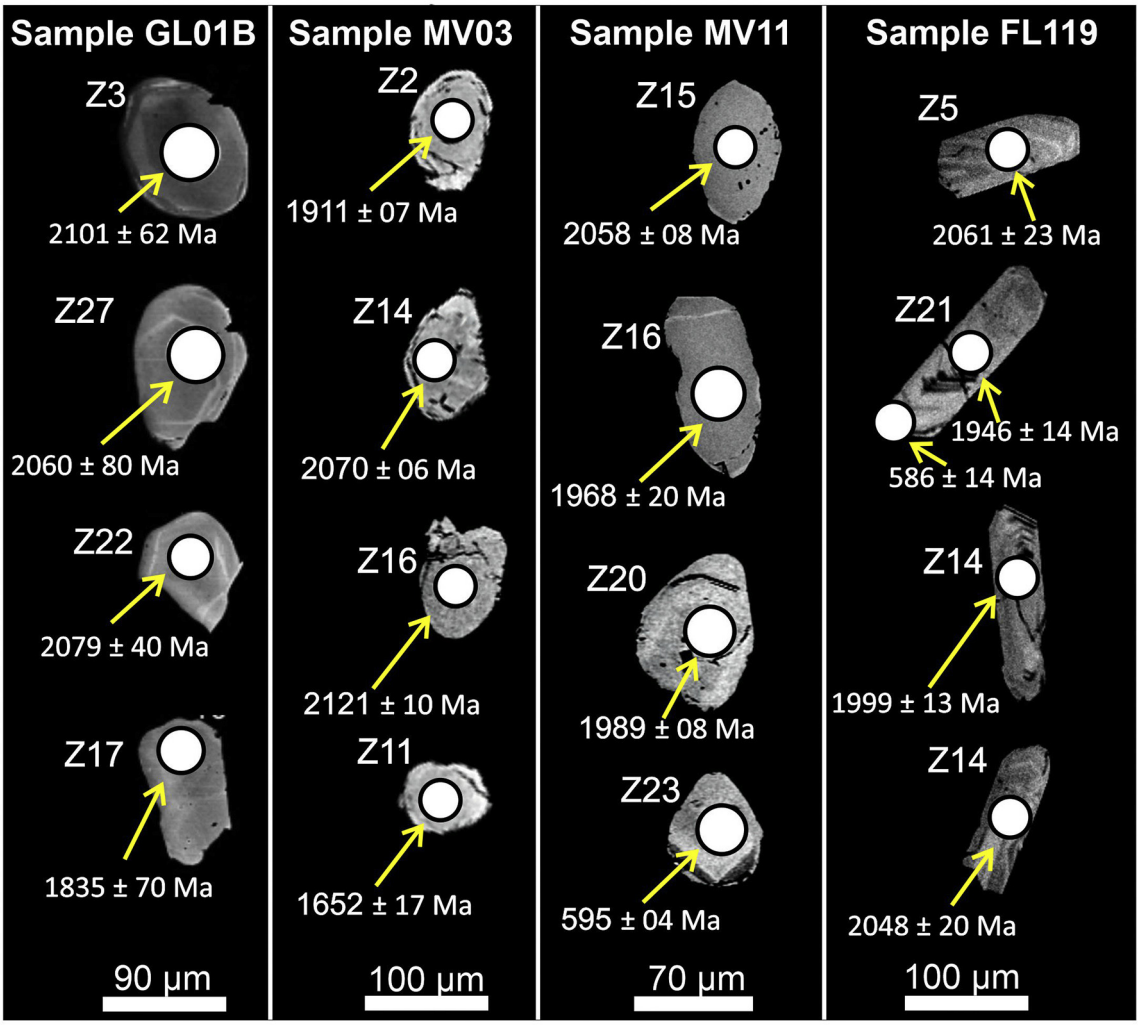

Fig. 4. Cathodoluminescence images from representative analyzed zircon crystals for U-Pb with the $^{207}Pb/^{235}U$ ages and spot position represented.

present (Fig. 4d). In addition, tiny crystals occupying the core of the major zircon grains are interpreted as inheritance from the host rocks. Fifty-eight crystals were analyzed, but due to their high discordance (>50%), only twenty-five analyzed spots were considered for the age calculation. An igneous origin is attributed to all the analyzed spots, which is grounded on the crystal morphologies, presence of well-developed oscillatory zoning and Th/U ratios ranging from 0.17 to 3.7. The concordia diagram yields an upper intercept age of 2076 ± 12 Ma (MSWD = 2.7), which is interpreted as the protolith age of the metamonzogranite, whereas the lower intercept yields an age of 574 ± 12 Ma, interpreted as the result of Pb loss during the Brasiliano metamorphism (Fig. 5d). A single xenocryst (Z15) aged at 2328 ± 49 Ma ($^{206}Pb/^{238}U$ age) is interpreted as the result of crustal inheritance.

4.2. Sm-Nd isotopes

Sm-Nd isotope analyses were performed on representative samples from both the Fazenda Carmo and Riacho do Navio suites, including those analyzed for zircon U-Pb. The only exception is sample MV11 due to its primitive nature. Rocks from the Fazenda Carmo Suite are characterized by T_{DM} model ages ranging from early Archean to early Paleoproterozoic (i.e., 3.34–2.25 Ga) and the calculated $\varepsilon_{Nd}(t)$ values using the crystallization age of 2.12 Ga are very similar to the CHUR and DM values, with a narrow range of +2.11 to −0.03, thus consistent with a juvenile origin (Fig. 6a). T_{DM} model ages for the Riacho do Navio Suite samples strongly resemble those from the Fazenda Carmo Suite, ranging from 2.90 to 2.20 Ga. In contrast, the obtained $\varepsilon_{Nd}(t)$ values using the 2.076 Ga crystallization age, range from slightly positive to strongly negative (i.e., +1.70 to −9.22), suggesting a dominant crustal component in the source region (Fig. 6b).

4.3. Whole-rock geochemistry

In terms of major elements, rocks of the Fazenda Carmo Suite are characterized by narrow ranges in most major elements, containing 42.6–52.4 wt.% SiO_2, 12.8–18.4 wt.% Al_2O_3, 9.2–13.2 wt.% CaO, 12.4–17.0 wt.% Fe_2O_3, 1.1–2.5 wt.% Na_2O, 0.3–0.6 wt.% K_2O. The calculated Mg# fluctuates between 26.2 and 39.5 and its precursor magma can be classified as tholeiitic on the AFM diagram (Fig. 7a). Major elements for the Riacho do Navio Suite samples present 69.5–75.9 wt.% SiO_2, 12.7–16.8 wt.% Al_2O_3, 0.75–2.12 wt.% CaO, 0.97–5.0 wt.% Fe_2O_3, 1.06–5.0 wt.% Na_2O and 4.0–5.8 wt.% K_2O. They plot near the line of the calc-alkaline series (Fig. 7a). Their protoliths share similarities with calc-alkalic and alkalic calcic (Fig. 7b) and ferroan magma series (Fig. 7c), as shown by plots on the diagrams by Frost et al. (2001), which are typical for Cordilleran granitic rocks. They are also classified as meta- to strongly peraluminous rocks, based on the plot of the A/CNK

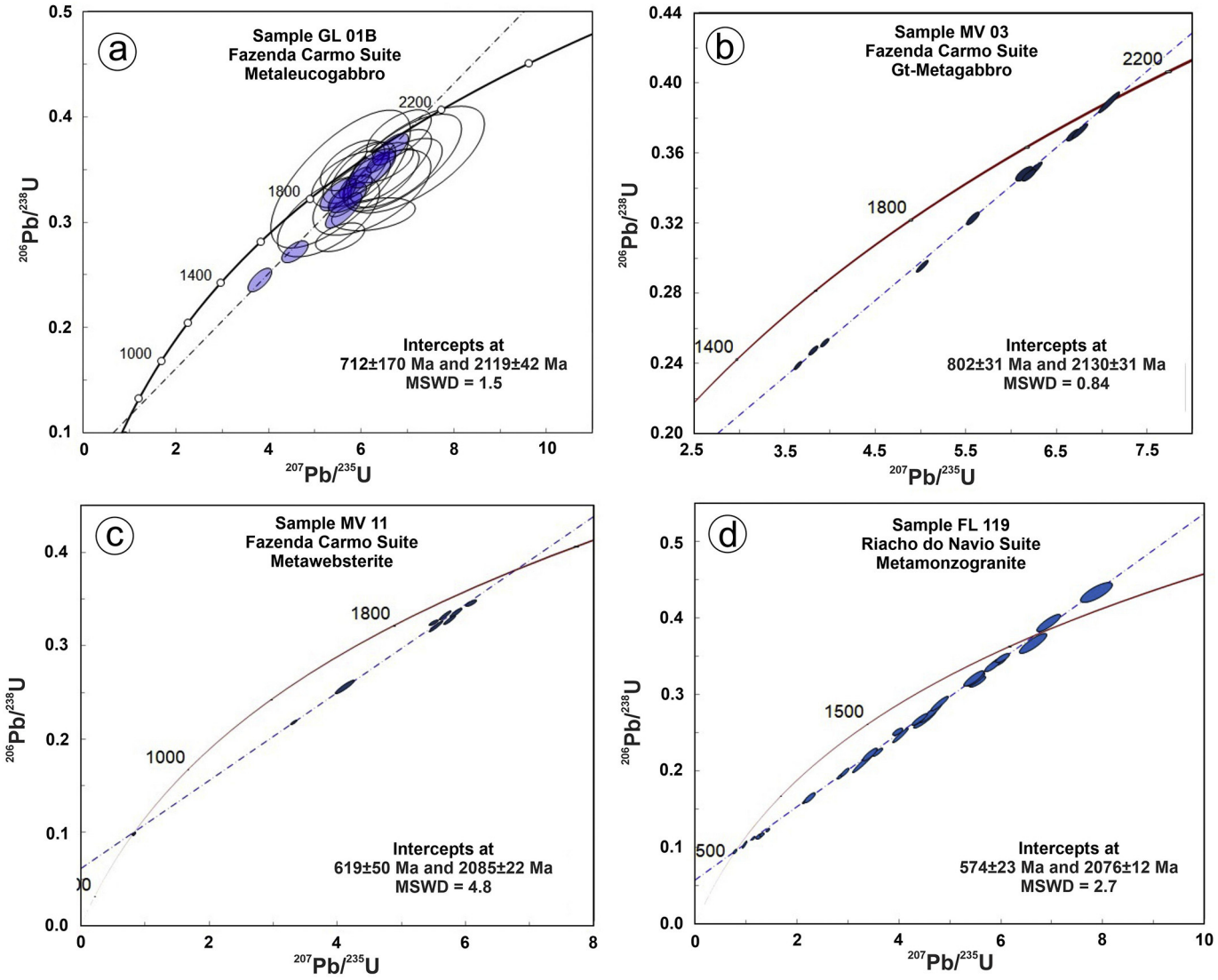

Fig. 5. U-Pb concordia diagrams for the U-Pb zircon analyzed samples.

[Al_2O_3/(Na_2O + K_2O) vs. Al_2O_3/(CaO + Na_2O + K_2O)] molar diagram from Maniar and Piccoli (1989) (Fig. 7d).

Considering the minor/trace element behavior, on the chondrite normalized multi-element/spider diagram, samples from the Fazenda Carmo Suite present positive and negative anomalies on both large ion lithophile elements (LILE) and high field strength elements (HFSE). Significant negative anomalies are observed on Rb, Nb, Zr and Hf, whereas Sr may fluctuate between negative to positive anomalies (Fig. 8a). In addition, the rare earth elements distribution normalized to chondritic values are homogeneous and the general pattern is relatively flat, with a weak enrichment of light rare earth elements (LREE) with respect to heavier rare earth elements (HREE) (La_N/Yb_N = 2.1–11.3). No anomalies are observed along the REE distribution, except for discrete troughs of Ce and elevated contents of Pr (Fig. 8b). On the other hand, rocks from the Riacho do Navio Suite present strong enrichment of LILE as compared to HFSE on the chondrite normalized multi-element/spider diagram, which is characterized by negative anomalies of Nb, Ta, Sr, P and Ti (Fig. 8c). The REE distribution normalized with chondritic values present strong enrichment of LREE compared with HREE (La_N/Yb_N = 17.8–141.6) and all samples have negative Eu anomalies (Eu/Eu* = 0.45–0.55; Fig. 8d).

In terms of tectonic discrimination diagrams, samples from the Fazenda Carmo Suite plot along the volcanic arc array on the Nb/Yb vs. Th/Yb diagram (Pearce, 2014; Fig. 9a) and present chemical compositions similar to basaltic rocks generated in continental arc-related settings (Fig. 9b and c). On the Hf–Rb/30–Ta × 3 ternary plot proposed by Harris et al. (1986), samples from the Riacho do Navio Suite plot in the volcanic arc field (Fig. 9d), whereas on the Ta vs. Yb diagram from Pearce et al. (1984), they are akin to volcanic-arc derived and collisional-related magmas (Fig. 9e). On the Al_2O_3/(FeO^t + MgO)–CaO–5(K_2O/Na_2O) triangular plot from Laurent et al. (2014), the samples of the Riacho do Navio Suite share similarities with magmas derived from melting of metasedimentary sources (Fig. 9f).

5. Discussion

5.1. Age, source and tectonic setting

The Fazenda Carmo Suite comprises a succession of metamafic and meta-ultramafic rock lenses along the ca. 2.1 Ga metagranites and orthogneisses of the Floresta Batholith (Santos et al., 2017a). Original igneous textures are obliterated at the meso- and micro-

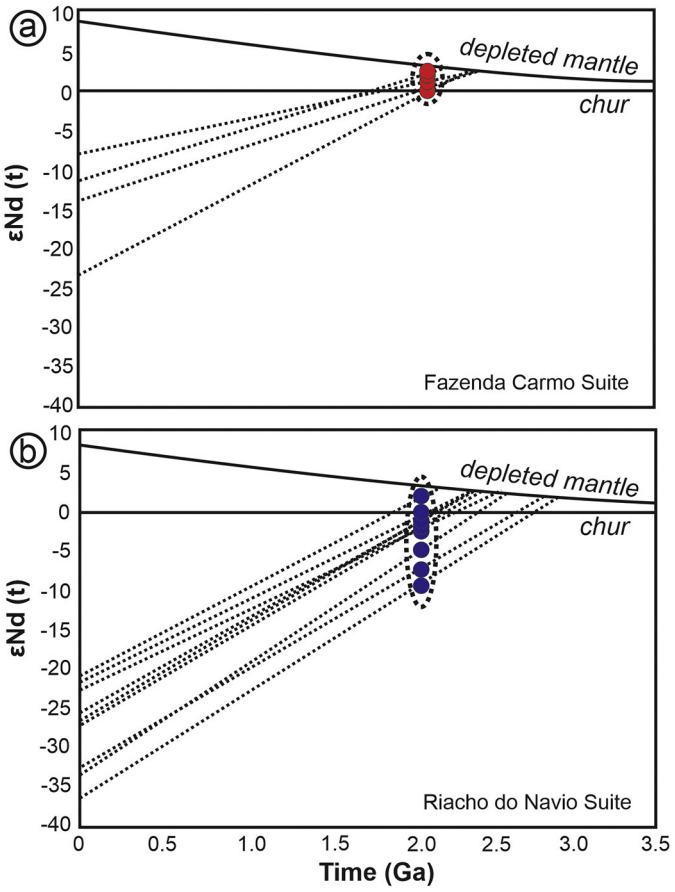

Fig. 6. Nd evolution diagram for the samples of the (a) Fazenda Carmo Suite and (b) Riacho do Navio Suite. Mantle evolution curve from DePaolo (1981).

scale due to the Neoproterozoic Brasiliano orogenesis overprint. Dated metamafic rocks yield ages at ca. 2.13 and 2.11 Ga, whilst a metawebsterite sample was dated at ca. 2.08 Ga. This is the first successful attempt to date an ultramafic lithotype via U-Pb zircon methodology within the Central Subprovince. Based on the primitive nature of the analyzed sample, we do not discard that this age might be attributed to crustal inheritance. However, all the analyzed zircon crystals present almost the same crystallization ages as compared with the metamafic protolith samples, besides similar morphology and absence of inherited nuclei, which is highly suggestive for crystals derived from the original magma. Nevertheless, we assume that more geochronological investigation is needed, especially on the metamafic-ultramafic sequences of the Alto Moxotó Terrane that have been neglected over the years.

The Riacho do Navio Suite is composed of metamonzogranites and orthogneisses that occur as sheeted-like intrusions with gently dipping foliation due to the influence of the Serra do Jabitacá Shear Zone. Based on our results, we suggest that the crystallization age of their protoliths is ca. 2.08 Ga and considering the analytical errors might be interpreted as coeval or slightly younger than rocks from the Fazenda Carmo Suite. Samples from both suites have lower intercept Neoproterozoic ages ranging between ca. 619 and 570 Ma (samples MV11 and RN02), consistent with the age of the Brasiliano orogenic event in the Borborema Province (650–540 Ma; Brito Neves et al., 2014).

Based on the $\varepsilon_{Nd}(t)$ values, we conclude that the Fazenda Carmo Suite samples are chondrite-like and compatible with extraction from a juvenile depleted mantle source (e.g., DePaolo and Wasserburg, 1976; Miller and Coleman, 1988) and reflect early Paleoproterozoic crustal growth within the Alto Moxotó Terrane. In addition, the overall geochemical characteristics of this suite point to a primitive or poorly evolved source (e.g., low values of LILE, HFSE and REE), despite little fractionation of the REE. Experimental studies suggest that the trace element distribution is akin to magmas generated by melting of a depleted mantle source (e.g., Prouteau et al., 2001; Grove et al., 2006). The conspicuous negative anomalies observed for Nb, Zr and Hf within the mafic-derived magmas are usually ascribed to the presence of rutile in a fluid-rich source, that might reflect some degree of upper mantle metasomatism (Brenan et al., 1994; Klemme et al., 2005). Indeed, such a scenario is commonly envisaged through partial melting of peridotites, triggered by the saturation of volatiles such as H_2O and CO_2 in the mantle wedge (e.g., Gaetani and Grove, 1998).

The tectonic discriminant diagrams indicate that the studied rocks are akin to arc-related continental basaltic magmas, marked by higher Th/Yb ratios compared with typical N-MORB or E-MORB values (Pearce, 2014). In addition, the characteristic higher La/Yb ratios observed in our samples (mostly higher than 1.4) are suggestive of crustal contamination, which is inevitable during magma ascent in continental arcs. We envisage that the mafic magmas were extracted from the mantle and emplaced in the lower crust during the ongoing of subduction (e.g., Condie, 1999).

Conversely, rocks from the Riacho do Navio Suite have negative $\varepsilon_{Nd}(t)$ values, which are compatible with crustal reworking in the source region. Major element behavior indicate that they share chemical similarities with calc-alkalic to alkali-calcic and ferroan magmas, being chemically similar to evolved Cordilleran granites (Frost et al., 2001). They are also meta- to strongly peraluminous, that can be explained by the presence of garnet and minor muscovite in their mineralogy. Trace element distribution is characterized by enrichment of LILE compared to HFSE, as well as Nb, Ta, P and Ti negative anomalies. This pattern might reflect, for instance, retention of these elements by sphene, rutile or Ti-bearing amphibole (Foley et al., 2000). The negative anomalies of the HFSE as well as the Cordilleran nature of the studied rocks are proxies for classical subduction-related magmas (e.g., McMillan et al., 1989; Barth et al., 2000). The HREE contents are very low as compared with LREE, which might reflect partitioning into garnet, whereas Eu anomalies are interpreted as retention of plagioclase in the source region. However, due to their strong pressure sensitiveness, these anomalies might indicate mixing of mantle and crustal sources (e.g., Hagen-Peter et al., 2015).

A subduction-related origin for the Riacho do Navio Suite is reinforced by their plots on discriminant diagrams, transitioning from arc-related to collisional-related magmas. They also present transition between meta- to strong peraluminous character (S-type granites) and based on the coeval obtained U-Pb age with the Floresta Batholith (mostly intermediate metaplutonic rocks with arc-related signature), it is possible that they can be part of the magmatic arc itself, being products of oceanic floor and arc-derived sandstones melting (Shaw and Flood, 1981). A second plausible alternative, is that rocks from the Riacho do Navio Suite might have been generated in a collisional setting (Pearce et al., 1984), in which the high Al_2O_3 contents may be interpreted as the result of upper crust melting, including high proportions of metasedimentary components (Chappell and White, 2001; Laurent et al., 2014), which is in concordance with their regional correlatives.

5.2. Toward a tectonic model for the Paleoproterozoic arc evolution of the Alto Moxotó Terrane

Recent isotopic and geochemical investigations conducted in distinct areas of the Central Borborema Province have outlined the importance of early Paleoproterozoic accretionary episodes,

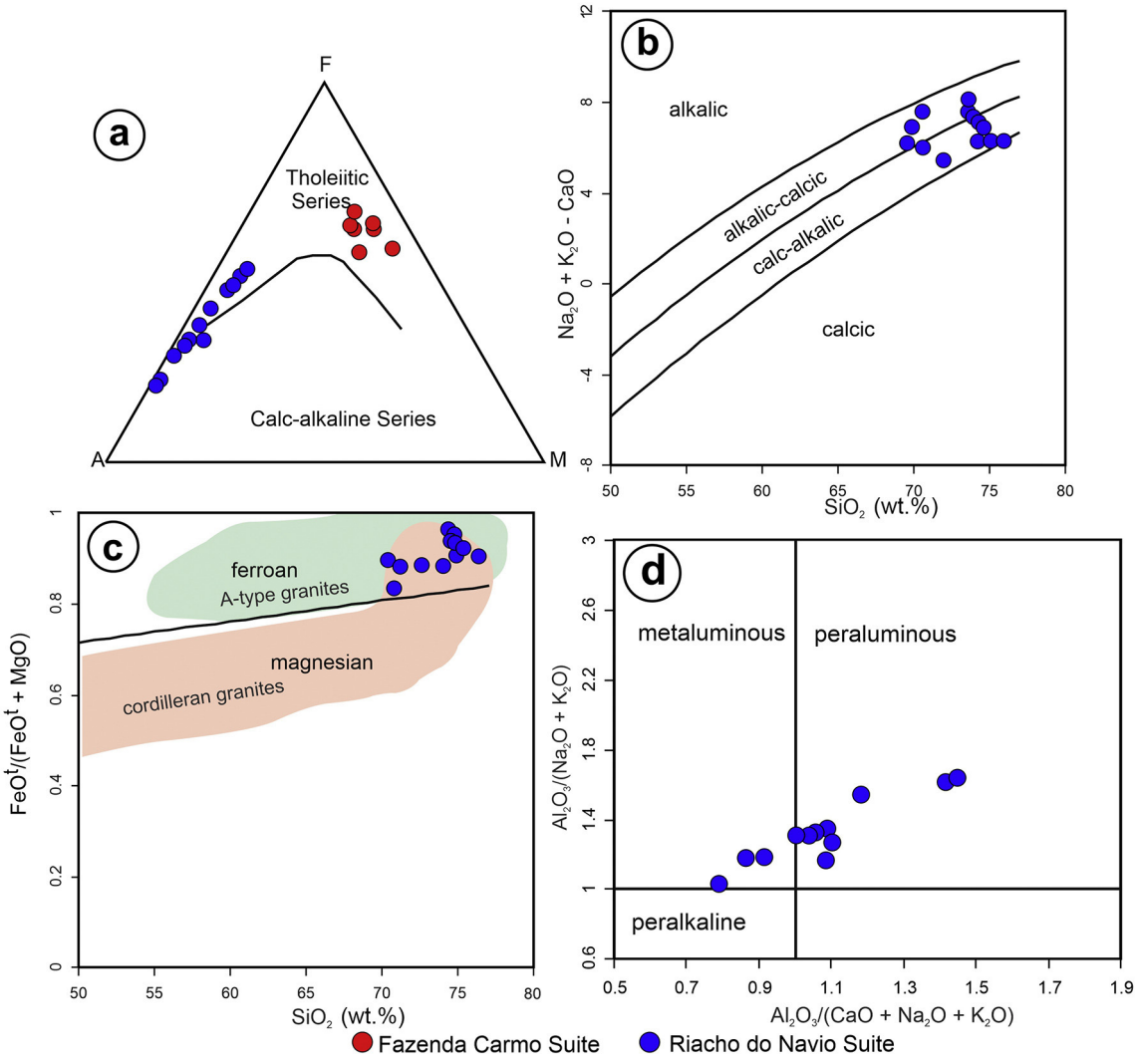

Fig. 7. Geochemical characteristics of the Fazenda Carmo and Riacho do Navio Suites. (a) AFM diagram from Irvine and Baragar (1971); (b) SiO_2 vs. $Na_2O + K_2O$ – CaO diagram from Frost et al. (2001); (c) SiO_2 vs. $FeO^t/(FeO^t + MgO)$ diagram from Frost et al. (2001); (d) A/CNK diagram molar diagram from Maniar and Piccoli (1989).

marking major sites of crustal growth and reworking (e.g., Neves et al., 2015; Santos et al., 2015). In addition, the recent discovery of juvenile TTG crustal segments within the Alto Moxotó Terrane aged at ca. 2.6 Ga (Santos et al., 2017a; Brito Neves and Silva Filho, 2020) as well as several Neo- and Mesoarchean inherited zircon crystals in supracurstal rocks (e.g., Santos et al., 2015) and ancient Nd T_{DM} model ages strongly indicate that Paleoproterozoic subduction might have occurred beneath a hidden Archean block (i.e., continental arc setting).

Continental arcs have a wide compositional range, including silica-poor stages associated with the early phases of convergent plate margin development to highly evolved magmas marking the subduction termination (Tatsumi and Stern, 2006). Mafic and ultramafic rocks from the Fazenda Carmo Suite represent relics of a primitive arc stage at ca. 2.1 Ga, in which tholeiitic magmas were generated by mantle wedge melting. Considering the coeval age of the typical cordilleran phase (i.e., the emplacement of the Floresta Batholith) and the emplacement of meta- to peraluminous magmas related to the Riacho do Navio Suite, the latter might have been generated during the ongoing subduction not necessarily involving a collisional episode, such as in the Terra Australis orogen (Cawood et al., 2011) in eastern Australia (Fig. 10a and b). Another possible scenario might be glimpsed considering a typical continental arc evolution (i.e., oceanic subduction-continental collision) and in such case, we suggest that the timing from subduction to collision might have lasted at least 100 Ma (Fig. 10c). In a short period of crustal growth, dominant Cordilleran magmatism was generated producing juvenile material, but also reworking Archean crust, marked by "arc batholiths" such as the Floresta Batholith (e.g., Ducea, 2001). In advanced stages of arc evolution, mantle melting is reduced and slab break-off is followed by continent-continent collision (Fig. 10d), resulting in upper crust partial melting (Chappell and White, 2001; Condie, 2007; Cawood et al., 2009).

Other displaced coeval arc segments might include supracrustal rocks of the Sertânia Complex, that yield a maximum depositional age at around ca. 1.97 Ga, as well as detritus from early Paleoproterozoic and late Archean sources, being the main candidate for a remnant of a retroarc-foreland basin within the Alto Moxotó Terrane. Furthermore, recently described ca. 1.97 Ga potassic rocks in the central portion of the Terrane might also mark advanced stages of continental crust stabilization, interpreted as the transition between *syn*- to post-collisional magmatism (Santos and Santos, 2019).

Lastly, the transition between the Rhyacian to Orosirian period is still not well understood both in South America and in the Bor-

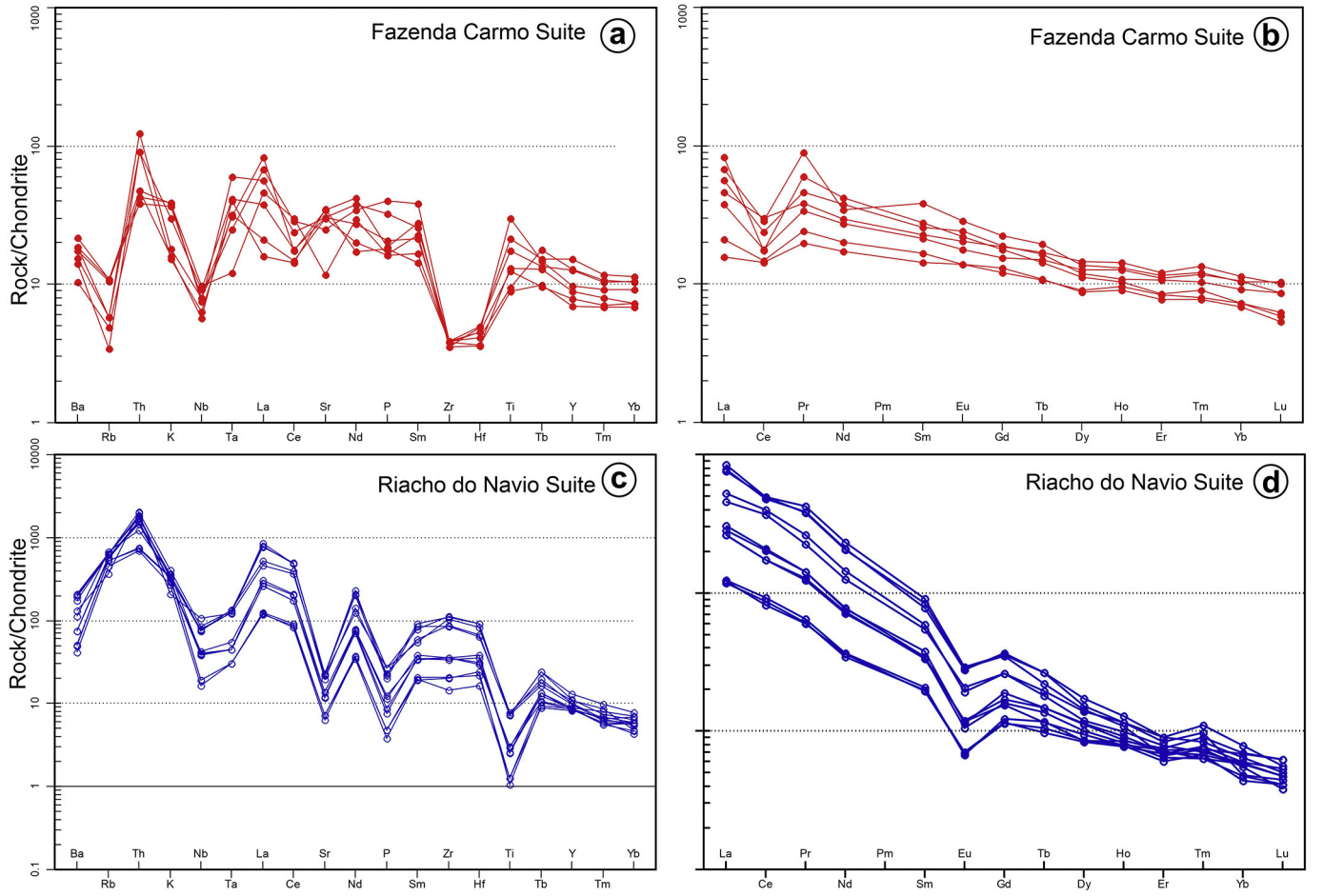

Fig. 8. (a) Spider diagram of trace element abundances for the Fazenda Carmo Suite samples; (b) Spider diagram of trace element abundances for the Riacho do Navio Suite samples; (c) REE abundances for the Fazenda Carmo; (d) REE abundances for the Riacho do Navio Samples. Spider diagrams were normalized by primitive mantle from McDonough and Sun (1995) and REE normalized by Chondrite from Nakamura (1974).

borema Province, and has received major attention because of its association with eclogite-granulitic metamorphic peaks, suggestive of suture development during the proposed period of arc activity (Santos et al., 2013a, 2013b; Neves et al., 2015). As shown by the distinct models proposed in this paper, the orogenic history of the Alto Moxotó Terrane during this period still needs additional data and investigation.

5.3. Regional correlations and implications for Proterozoic paleocontinents

In West Gondwana, a number of early to late Paleoproterozoic orogenic belts are recognized, mostly concentrated in the cratons, such as the São Francisco-Congo and São Luis-West Africa blocks (Alkmim and Marshak, 1998; Ennih and Liégeois, 2008; Klein and Moura, 2008). They are characterized by a protracted accretionary tectono-magmatic evolution with major crustal growth period recorded at ca. 2.1 Ga, related to the assembly of Paleo- to Neoarchean microcontinents (e.g., Heilbron et al., 2017). Breakup of the early landmasses is well-marked by several dyke swarms that are dated at ca. 1.9 Ga, 1.8–1.7 Ga, 1.6–1.5 Ga and 1.0–0.9 Ga (Ernst et al., 2013; Caxito et al., 2020). Paleoproterozoic crust within them present evidence for a variety of tectono-magmatic scenarios, including remnants of TTG, sanukitoid and greenstone-like mafic-ultramafic sequences as well as island- to continental arcs, including voluminous calc-alkaline to highly peraluminous granite emplacement (e.g., Barbosa and Sabaté, 2004; Batumike et al., 2009; Ávila et al., 2010).

The Neoproterozoic orogens of South America and West Africa resulted from the assembly of West Gondwana and their inner Paleoproterozoic domains are mostly disrupted, being interpreted as exotic terranes or basement inliers (Brito Neves, 2011 and references therein). Despite the strong overprint of the Brasiliano deformation and metamorphism in the Borborema Province, coeval Paleoproterozoic blocks have been long recognized in all subprovinces as well as in the São Francisco Craton (Fig. 11).

A similar accretionary scenario proposed in this paper has been speculated within the Alto Moxotó Terrane (e.g., Santos et al., 2012, 2013a, 2013b, 2015), but links between early arc formation and later compression were missing (Santos et al., 2017a). Herein, we have revealed the former products, the tholeiitic Fazenda Carmo Suite, to be the result of early subduction, which is coeval to other poorly understood mafic-ultramafic sequences within basement units of the Central Subprovince (e.g., Neves et al., 2015; Santos et al., 2015). A remarkable Paleoproterozoic unit of the Alto Moxotó Terrane is the calc-alkaline ca. 2.1 Ga Floresta Batholith that outcrops in the studied region, corresponding to a major Cordilleran arc-related magmatic record in the region (Santos et al., 2017a), and we interpret the 2.08 Ga Riacho do Navio Suite as part of this subduction-related complex.

Coeval arc-related settings within the Borborema Province span from ca. 2.2 to 2.1 Ga (e.g., Souza et al., 2007; Neves et al., 2015), that clearly fits with the age interval of the Transamazonian-

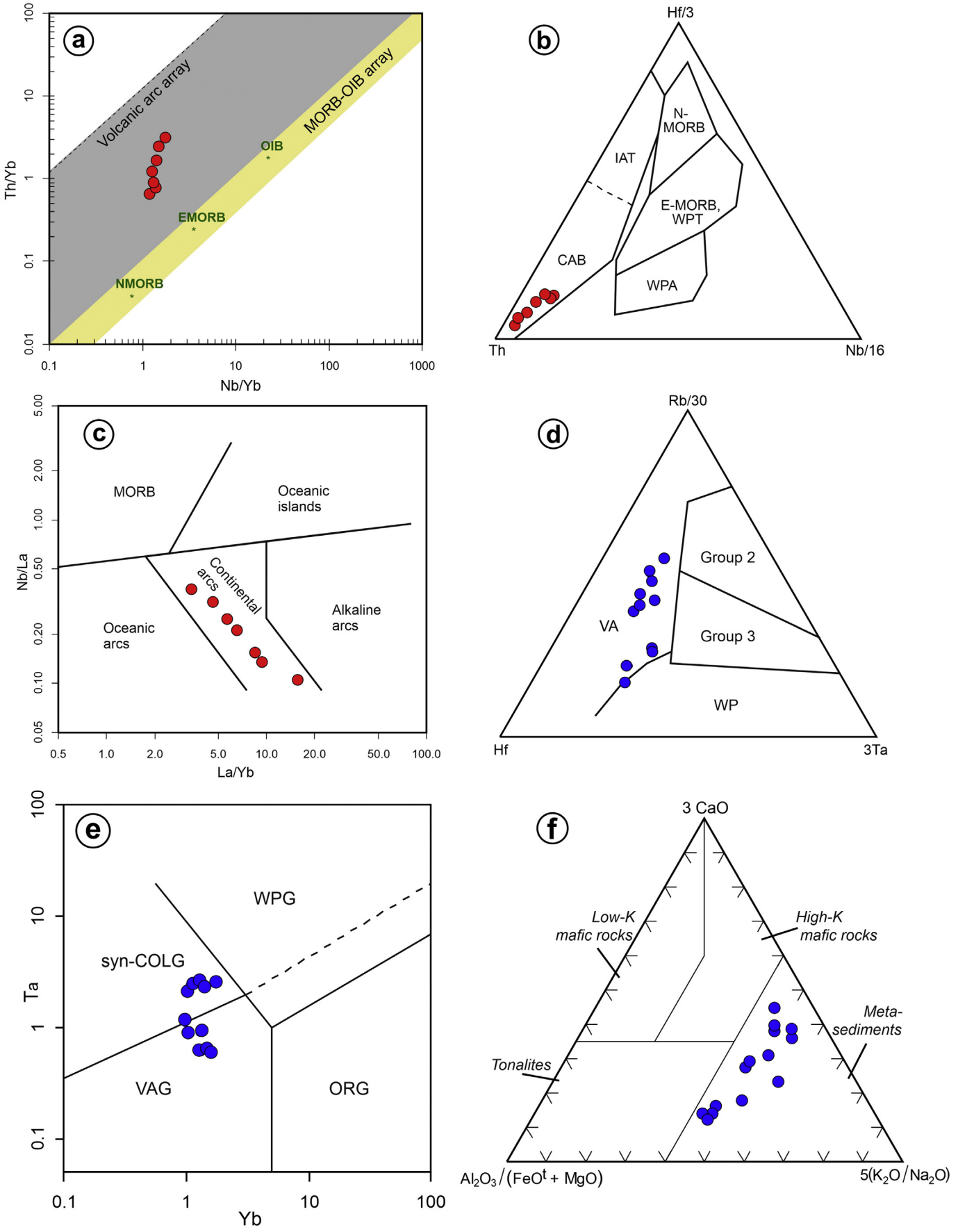

Fig. 9. Tectonic discriminant diagrams for the studied units. (a) Nb/Yb vs. Th/Yb diagram (Pearce, 2014); (b) Th–Hf/3–Nb/16 ternary plot from Wood (1980); (c) La/Yb vs. Nb/La diagram from Hollocher et al. (2012); (d) Hf–Rb/30–Ta × 3 ternary plot proposed by Harris et al. (1986); (e) Ta vs. Yb diagram from Pearce et al. (1984); (f) Al_2O_3/(FeO^t + MgO)–3CaO–5(K_2O/Na_2O) triangular plot from Laurent et al. (2014). Symbols are the same as Fig. 7.

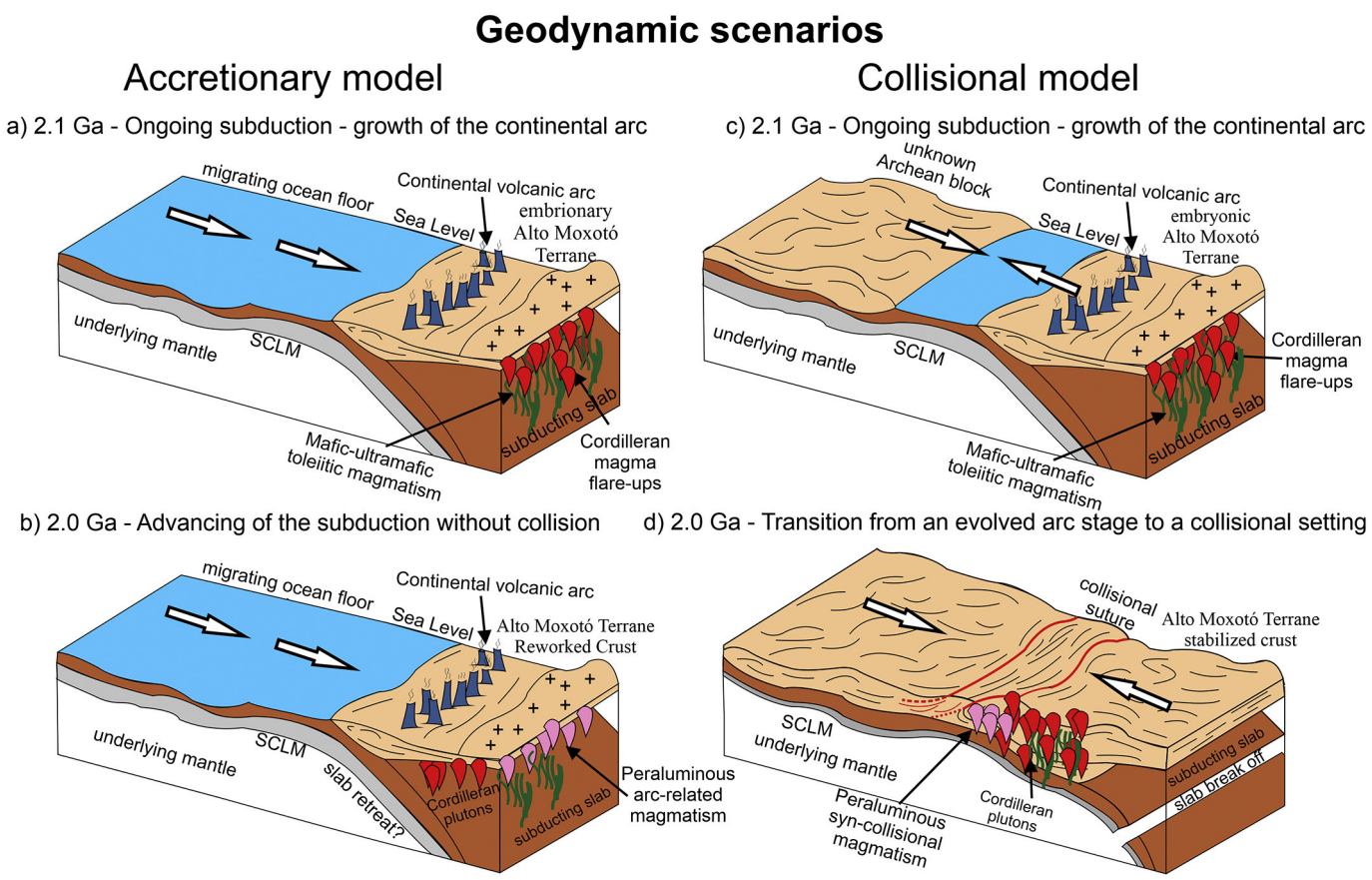

Fig. 10. Possible tectonic scenarios for the Alto Moxotó Terrane evolution based on this study.

Eburnian orogeny. Additional elements of accretionary tectonics in this period also include a possible ca. 1.96 Ga supra-subduction zone ophiolite or island-arc tholeiite remnants in the Southern Subprovince (Caxito et al., 2015), detrital material of continental magmatic arc exhumation (e.g., Caxito et al., 2014a, 2014b; Lima et al., 2018, 2019), and eclogitic and retro-eclogitic assemblages recorded in the Central Subprovince (Almeida et al., 2009; Santos et al., 2012, 2013a, 2013b).

In the Pan-African orogenic belts, relics of Archean and Paleoproterozoic accretionary episodes are well marked and also strongly reworked during the Pan-African orogeny (e.g., Toteu et al., 2001). The major markers include subduction-related TTG and normal calc-alkaline magmas as well as evidence of high-grade metamorphism related to collisional episodes at ca. 2.03 Ga (Penaye et al., 2004), interpreted as relics of Paleoproterozoic sutures, for instance, in southern Cameroon (Tsoungui et al., 2020).

The recognition of Paleoproterozoic growth and reworking markers within younger belts of West Gondwana has a critical role on paleogeographic speculations, especially concerning older supercontinents such as Columbia or Nuna. Indeed, some authors have already postulated that early Paleoproterozoic blocks such as the Alto Moxotó Terrane might represent missing pieces (e.g., Brito Neves and Silva Filho, 2020) of those supercontinents, presenting several similarities with the adjoining cratons of the Borborema Province, possibly extruded during the Neoproterozoic tectonics, being later docked along continental margins as exotic terranes.

6. Conclusions

(1) Zircon U-Pb data indicate that mafic-ultramafic and granitic magmatism was emplaced in the continental crust of the Alto Moxotó Terrane at ca. 2.13 and 2.08 Ga, respectively.

(2) Nd T_{DM} model ages suggest extraction from Mesoarchean to Paleoproterozoic sources, but mafic magmatism resulted from peridotite melting in a mantle wedge later contaminated by the continental crust, whereas the metagranitic rocks where derived from a sedimentary/metasedimentary source.

(3) The overall geochemistry suggests that the studied rocks are part of a large magmatic spectrum generated in a continental arc-related setting, in which tholeiitic magma was emplaced in an early stage of subduction and meta- to peraluminous material resulted from crust melting during the convergence termination, thus marking the end of the orogenic activity within the Alto Moxotó Terrane during the Paleoproterozoic.

(4) The obtained results as well as several investigations that were carried out in the terrane in recent years suggest that it corresponds to a *quasi*-rigid block located in the interior of the Neoproterozoic Borborema Province, being a possible candidate for a dismembered fragment of the Nuna/Columbia Supercontinent.

Declaration of competing interest

The authors declare that they have no known competing financial interests or personal relationships that could have appeared to influence the work reported in this paper.

Acknowledgements

This paper represents a later contribution of the first author PhD thesis. PAC acknowledges support from Australian Research

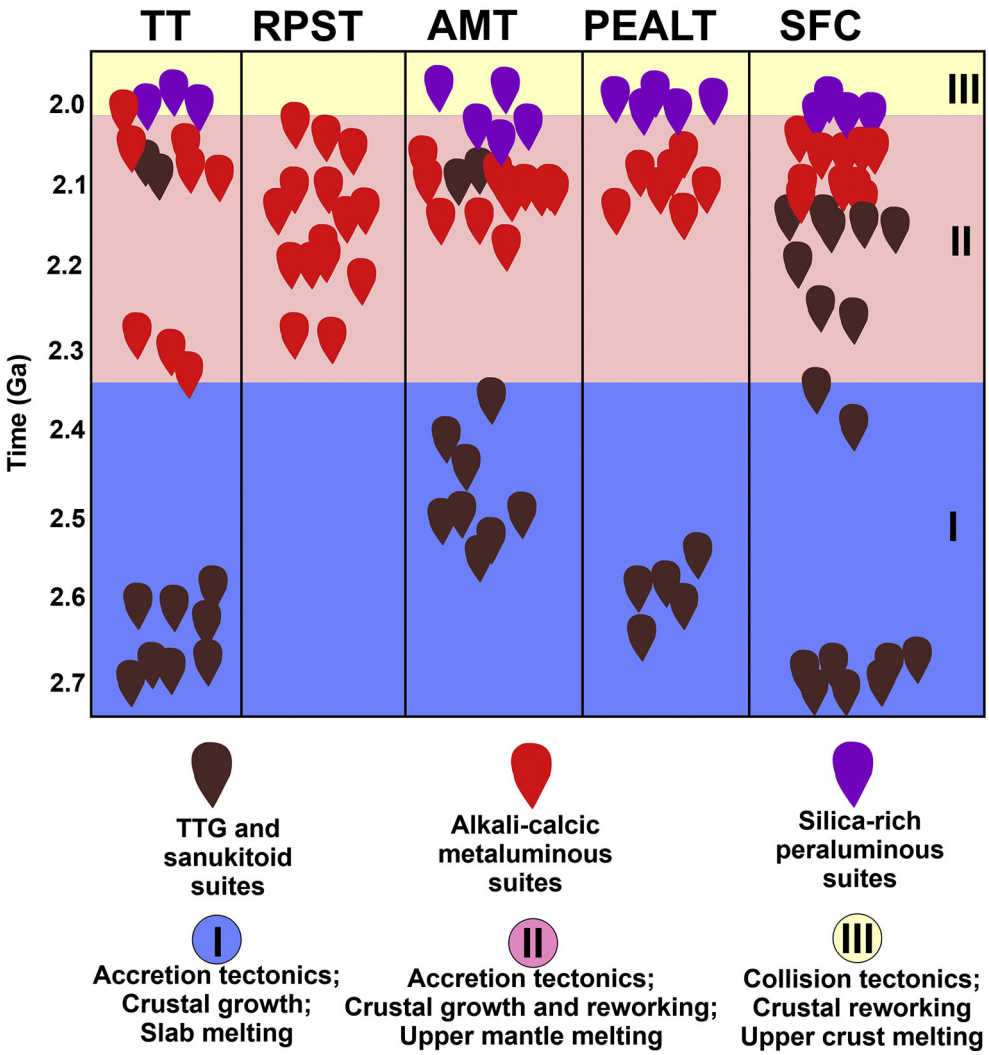

Fig. 11. Correlation between the main late Archean and early Paleoproterozoic crustal events of the Alto Moxotó Terrane (AMT), other basement domains of the Borborema Province and the São Francisco Craton (SFC). Northern Subprovince: TT–Tróia Terrane, RPST–Rio Piranhas-Seridó Terrane; Southern Subprovince terrane: PEALT–Pernambuco-Alagoas Terrane. Crystallization ages was compiled from Hollanda et al. (2011), Sá et al. (2014), Costa et al. (2015, 2018), Neves et al. (2015), Santos et al. (2017a), Brito Neves and Silva Filho (2020), Bruno et al. (2020) and references therein.

Council grant FL160100168. This study was supported by the National Institute of Science and Technology for Tectonic Studies (INCT) of Brazil. Comments and criticism made by Dr. Henrique Bruno and an anonymous reviewer are appreciated as well as those from Kathryn Cutts and M. Santosh.

References

Alkmim, F.F., Marshak, S., 1998. Transamazonian Orogeny in the Southern São Francisco Craton Region, Minas Gerais, Brazil: evidence for Paleoproterozoic collision and collapse in the Quadrilátero Ferrífero. Precambrian Res. 90, 29–58. https://doi.org/10.1016/s0301-9268(98)00032-1.

Almeida, F.F.M., Hasui, Y., de Brito Neves, B.B., Fuck, R.A., 1981. Brazilian structural provinces: an introduction. Earth-Sci. Rev. 17, 1–29. https://doi.org/10.1016/0012-8252(81)90003-9.

Almeida, C.N., Guimarães, I.P., Beurlen, H., Topitsch, W.M., Ferrer, D.M.M., 2009. Evidências de metamorfismo de alta pressão na faixa de dobramentos Pajeú – Paraíba, Província Borborema, nordeste do Brasil: petrografia e química mineral de rochas metamáficas. Rev. Bras. de Geoc. 29, 421–434. https://doi.org/10.25249/0375-7536.2009394421434 (in Portuguese).

Ávila, C.A., Teixeira, W., Cordani, U.G., Moura, C.A.V., Pereira, R.M., 2010. Rhyacian (2.23-2.20 Ga) juvenile accretion in the southern São Francisco craton, Brazil: Geochemical and isotopic evidence from the Serrinha magmatic suite, Mineiro belt. J. South Am. Earth Sci. 29, 464–482. https://doi.org/10.1016/j.jsames.2009.07.009.

Barbosa, J.S.F., Sabaté, P., 2004. Archean and Paleoproterozoic crust of the São Francisco Craton, Bahia, Brazil: geodynamic features. Precambrian Res. 133, 1–27. https://doi.org/10.1016/j.precamres.2004.03.001.

Barth, M.G., McDonough, W.F., Rudnick, R.L., 2000. Tracking the budget of Nb and Ta in the continental crust. Chem. Geol. 165, 197–213. https://doi.org/10.1016/S0009-2541(99)00173-4.

Batumike, J.M., Griffin, W.L., O'Reilly, S.Y., Belousova, E.A., Pawlitschek, M., 2009. Crustal evolution in the Central Congo-Kasai Craton, Luebo, D.R. Congo: Insights from zircon U-Pb ages, Hf-isotope and trace-element data. Precambrian Res. 170, 107–115. https://doi.org/10.1016/j.precamres.2008.12.001.

Brenan, J.M., Shaw, H.F., Phinney, D.L., Ryerson, F.J., 1994. Rutile-aqueous fluid partitioning of Nb, Ta, Hf, Zr, U and Th: implications for high field strength element depletions in island-arc basalts. Earth Planet. Sci. Lett. 128, 327–339. https://doi.org/10.1016/0012-821X(94)90154-6.

Brito Neves, B.B., 2011. The Paleoproterozoic in the South-American continent: diversity in the geologic time. J. South Am. Earth Sci. 32, 270–286. https://doi.org/10.1016/j.jsames.2011.02.004.

Brito Neves, B.B., Silva Filho, A.F., 2020. O Superterreno Pernambuco-Alagoas na Província Borborema: ensaio de regionalização tectônica. Geo. USP - Sér. Cient. 18, 3–28. 11606/issn.2316–9095.v19–148257 (in Portuguese).

Brito Neves, B.B., Santos, E.J., Schmus, W.R.Q., 2000. Tectonic history of the Borborema Province. In: Cordani, U., Milani, E.J., Filho, A.T., de Almeida Campos, D. (Eds.), Tectonic Evolution of South America Rio de Janeiro: 31st International Geological Congress, Special Publication, pp. 151–182.

Brito Neves, B.B., Fuck, R.A., Pimentel, M.M., 2014. The Brasiliano collage in South America: a review. Braz. J. Geol. 44 (3), 493–518. https://doi.org/10.5327/Z2317-4889201400030010.

Brito Neves, B.B., Santos, E.J., Fuck, R.A., Santos, L.C.M.L., 2016. A preserved early Ediacaran magmatic arc at the northernmost portion of the Transversal Zone

central subprovince of the Borborema Province, Northeastern South America. Braz. J. Geol. 46 (4), 491–508. https://doi.org/10.1590/2317-4889201620160004.

Bruno, H., Elizeu, V., Heilbron, N., Valeriano, C.M., Strachan, R., Fowler, M., Bersan, S., Moreira, H., Dussin, I., Silva, L.G.E., Tupinambá, M., Almeida, J., Neto, C., Storey, C., 2020. Neoarchean and Rhyacian TTG-Sanukidoid suites in the southern São Francisco Paleocontinent, Brazil: evidence for diachronous change towards modern tectonics. Geosci. Front. 12, 1763–1787. https://doi.org/10.1016/j.gsf.2020.01.015.

Bühn, B.M., Pimentel, M.M., Matteini, M., Dantas, E.L., 2009. High spatial resolution analysis of Pb and U isotopes for geochronology by laser ablation multicollector inductively coupled plasma mass spectrometry (LA-MC-ICP-MS). An. Acad. Bras. Ciênc. 81, 1–16. https://doi.org/10.1590/S0001-37652009000100011.

Cawood, P.A., Kröner, A., Collins, W.J., Kusky, T.M., Mooney, W.D., Windley, B.F., 2009. Accretionary orogens through Earth history. Geol. Soc. Spec. Publ. 318, 1–36. https://doi.org/10.1144/SP318.1.

Cawood, P.A., Leitch, E.C., Merle, R.E., Nemchin, A.A., 2011. Orogenesis without collision: stabilizing the Terra Australis accretionary orogen, eastern Australia. Geol. Soc. Am. Bull. 123, 224–2255. https://doi.org/10.1130/B30415.1.

Cawood, P.A., Hawkesworth, C.J., Pisarevsky, S.A., Dhuime, B., Capitanio, F.A., Nebel, O., 2018. Geological archive of the onset of plate tectonics. Phil. Trans. Royal Soc. A 376, 2132. https://doi.org/10.1098/rsta.2017.0405.

Caxito, F.A., Uhlein, A., Stevenson, R., Uhlein, G.J., 2014a. Neoproterozoic oceanic crust remnants in Northeast Brazil. Geology 42, 387–390. https://doi.org/10.1130/G35479.1.

Caxito, F.A., Dantas, E.L., Stevenson, R., Uhlein, A., 2014b. Detrital zircon (U-Pb) and Sm-Nd isotope studies of the provenance and tectonic setting of basins related to collisional orogens: the case of the Rio Preto fold belt on the Northwest São Francisco Craton margin, NE Brazil. Gondwana Res. 26, 741–754. https://doi.org/10.1016/j.gr.2013.07.007.

Caxito, F.A., Uhlein, A., Dantas, E.L., Stevenson, R., Pedrosa-Soares, A.C., 2015. Orosirian (ca. 1.96 Ga) mafic crust of the northwestern São Francisco Craton margin: petrography, geochemistry and geochronology of amphibolites from the Rio Preto fold belt basement, NE Brazil. J. South Am. Earth Sci. 59, 95–111. https://doi.org/10.1016/j.jsames.2015.02.003.

Caxito, F.A., Uhlein, A., Dantas, E.L., Stevenson, R., Salgado, S.S., Dussin, I.A., da Sial, A. N., 2016. A complete Wilson Cycle recorded within the Riacho do Pontal Orogen, NE Brazil: implications for the neoproterozoic evolution of the Borborema Province at the heart of West Gondwana. Precambrian Res. 282, 97–120. https://doi.org/10.1016/j.precamres.2016.07.001.

Caxito, F.A., Hagemann, S., Dias, T.G., Barrote, V., Dantas, E.L., Oliveira, A.C., Campello, M.S., Campos, F.C., 2020. A magmatic barcode for the São Francisco Craton: Contextual in-situ SHRIMP U Pb baddeleyite and zircon dating of the Lavras, Pará de Minas and Formiga dyke swarms and implications for Columbia and Rodinia reconstructions. Lithos 374–375, 10578. https://doi.org/10.1016/j.lithos.2020.105708.

Caxito, F.A., Basto, C.F., Santos, L.C.M.L., Dantas, E.L., Medeiros, V.C., Gonçalves Dias, T., Barrote, V., Hagemann, S., Almim, A.R., Lana, C., 2021. Neoproterozoic magmatic arc volcanism in the Borborema Province, NE Brazil: possible flare-ups and lulls and implications for western Gondwana assembly. Gondwana Res. 91, 1–25. https://doi.org/10.1016/j.gr.2020.11.015.

Chappell, B.W., White, A.J.R., 2001. Two contrasting granite types: 25 years later. Aust. J. Earth Sci. 48, 489–499. https://doi.org/10.1046/j.1440-0952.2001.00882.x.

Condie, K.C., 1999. Mafic crustal xenoliths and the origin of the lower continental crust. Lithos 46, 95–101. https://doi.org/10.1016/s0024-4937(98)00056-5.

Condie, K.C., 2007. Accretionary orogens in space and time. Memoir Geol. Soc. Am. 200, 145–158. https://doi.org/10.1130/2007.1200(09).

Condie, K.C., Pisarevsky, S.A., Korenaga, J., Gardoll, S., 2015. Is the rate of supercontinent assembly changing with time? Precambrian Res. 259, 278–289. https://doi.org/10.1016/j.precamres.2014.07.015.

Costa, F.G., de Palheta, E.S.M., Rodrigues, J.B., Gomes, I.P., Vasconcelos, A.M., 2015. Geochemistry and U-Pb zircon ages of plutonic rocks from the Algodões granite-greenstone terrane, Troia Massif, northern Borborema Province, Brazil: implications for Paleoproterozoic subduction-accretion processes. J. South Am. Earth Sci. 59, 45–68. https://doi.org/10.1016/j.jsames.2015.01.007.

Costa, F.G., Klein, E.L., Lafon, J.M., Milhomem Neto, J.M., Galarza, M.A., Rodrigues, J. B., Naleto, J.L.C., Corrêa Lima, R.G., 2018. Geochemistry and U–Pb–Hf zircon data for plutonic rocks of the Troia Massif, Borborema Province, NE Brazil: evidence for reworking of Archean and juvenile Paleoproterozoic crust during Rhyacian accretionary and collisional tectonics. Precambrian Res. 311, 167–194. https://doi.org/10.1016/j.precamres.2018.04.008.

D'Agrella-Filho, M.S., Bispo-Santos, F., Trindade, R.I.F., Antonio, P.Y.J., 2016. Paleomagnetism of the Amazonian Craton and its role in paleocontinents. Braz. J. Geol. 46 (2), 275–299. https://doi.org/10.1590/2317-4889201620160055.

Damian Nance, R., Brendan Murphy, J., 2013. Origins of the supercontinent cycle. Geosci. Front. 4, 439–448. https://doi.org/10.1016/j.gsf.2012.12.007.

de Caxito, F.A., Santos, L.C.M.L., Ganade, C.E., Bendaoud, A., Fettous, E.-H., Bouyo, M. H., 2020. Toward an integrated model of geological evolution for NE Brazil-NW Africa: the Borborema Province and its connections to the Trans-Saharan (Benino-Nigerian and Tuareg shields) and Central African orogens. Braz. J. Geol. 502,. https://doi.org/10.1590/2317-4889202020190122 e20190122.

DePaolo, D.J., 1981. Nd isotopic studies: some new perspectives on Earth structure and evolution. EOS 62, 137–145. https://doi.org/10.1029/EO062i014p00137-01.

De Waele, B., Johnson, S.P., Pisarevsky, S.A., 2008. Palaeoproterozoic to Neoproterozoic growth and evolution of the eastern Congo Craton: its role in the Rodinia puzzle. Precambrian Res. 160, 127–141. https://doi.org/10.1016/j.precamres.2007.04.020.

DePaolo, D.J., Wasserburg, G.J., 1976. Nd isotopic variations and petrogenetic models. Geophys. Res. Lett. 3 (5), 249–252. https://doi.org/10.1029/GL003i005p00249.

Ducea, M., 2001. The California arc: thick granitic batholiths, eclogitic residues, lithospheric-scale thrusting, and magmatic flare-ups. GSA Today 11, 4–10. https://doi.org/10.1130/1052-5173(2001)011<0004:TCATGB>2.0.CO;2.

Ennih, N., Liégeois, J.P., 2008. The boundaries of the West African craton, with special reference to the basement of the Moroccan metacratonic Anti-Atlas belt. Geol. Soc. Spec. Publ. 297, 1–17. https://doi.org/10.1144/SP297.1.

Ernst, R.E., Pereira, E., Hamilton, M.A., Pisarevsky, S.A., Rodriques, J., Tassinari, C.C.G., Teixeira, W., Van-Dunem, V., 2013. Mesoproterozoic intraplate magmatic "barcode" record of the Angola portion of the Congo Craton: newly dated magmatic events at 1505 and 1110Ma and implications for Nuna (Columbia) supercontinent reconstructions. Precambrian Res. 230, 103–118. https://doi.org/10.1016/j.precamres.2013.01.010.

Ferreira, A.C.D., Dantas, E.L., Fuck, R.A., Nedel, I.M., 2020. Arc accretion and crustal reworking from late Archean to Neoproterozoic in Northeast Brazil. Sci. Rep. 10, 7855. https://doi.org/10.1038/s41598-020-64688-9.

Fetter, A.H., van Schmus, W.R., Santos, T.J.S., Nogueira Neto, J.A., Arthaud, M.H., 2000. U-Pb and Sm-Nd geochronological constraints on the crustal evolution and basement architecture of Ceará State, NW Borborema Province, NE Brazil: implications for the existence of the Paleoproterozoic Supercontinent "Atlantica". Rev. Bras. de Geoc. 3, 102–106. https://doi.org/10.25249/0375-7536.2000301102106.

Foley, S.F., Barth, M.G., Jenner, G.A., 2000. Rutile/melt partition coefficients for trace elements and an assessment of the influence of rutile on the trace element characteristics of subduction zone magmas. Geochim. Cosmochim. Acta 64, 933–938. https://doi.org/10.1016/S0016-7037(99)00355-5.

Frost, B.R., Barnes, C.G., Collins, W.J., Arculus, R.J., Ellis, D.J., Frost, C.D., 2001. A geochemical classification for granitic rocks. J. Petrol. 42, 2033–2048. https://doi.org/10.1093/petrology/42.11.2033.

Gaetani, G.A., Grove, T.L., 1998. The influence of water on melting of mantle peridotite. Contrib. Mineral. Petrol. 131 (4), 323–346. https://doi.org/10.1007/s004100050396.

Ganade de Araujo, C.E., Rubatto, D., Hermann, J., Cordani, U.G., Caby, R., Basei, M.A.S., 2014a. Ediacaran 2,500-km-long synchronous deep continental subduction in the West Gondwana Orogen. Nat. Commun. 5, 5198. https://doi.org/10.1038/ncomms6198.

Ganade de Araujo, C.E., Weinberg, R.F., Cordani, U.G., 2014b. Extruding the Borborema Province (NE-Brazil): a two-stage Neoproterozoic collision process. Terra Nova 26 (2), 157–168. https://doi.org/10.1111/ter.12084.

Gioia, S.M.C.L., Pimentel, M.M., 2000. The Sm-Nd isotopic method in the geochronologylaboratory of the University of Brasília. An. Acad. Bras. Cienc. 72, 219–245. https://doi.org/10.1590/S0001-37652000000200009.

Grove, T.L., Chatterjee, N., Parman, S.W., Médard, E., 2006. The influence of H_2O on mantle wedge melting. Earth Planet. Sci. Lett. 249, 74–89. https://doi.org/10.1016/j.epsl.2006.06.043.

Hagen-Peter, G., Cottle, J.M., Tulloch, A.J., Cox, S.C., 2015. Mixing between enriched lithospheric mantle and crustal components in a short-lived subduction-related magma system, Dry Valleys area, Antarctica: insights from U-Pb geochronology, Hf isotopes, and whole-rock geochemistry. Lithosphere 7 (2), 174–188. https://doi.org/10.1130/L384.1.

Harris, N.B.W., Pearce, J.A., Tindle, A.G., 1986. Geochemical characteristics of collision-zone magmatism. Geol. Soc. Spec. Publ. 19, 67–81. https://doi.org/10.1144/GSL.SP.1986.019.01.04.

Hawkesworth, C.J., Cawood, P.A., Dhuime, B., Kemp, T.I.S., 2017. Earth's continental lithosphere through time. Annu. Rev. Earth Planet Sci. 45, 169–198. https://doi.org/10.1146/annurev-earth-063016-020525.

Heilbron, M., Cordani, U.G., Alkmim, F.F., 2017. The São Francisco craton and its margins. In: Heilbron, M., Cordani, U., Alkmim, F. (Eds.), São Francisco Craton, Eastern Brazil, Tectonic Genealogy of a Miniature Continent. Regional Geology Reviews. Springer, Cham, pp. 3–13. https://doi.org/10.1007/978-3-319-01715-0_1.

Hollanda, M.H.B.M., Archanjo, C.J., Souza, L.C., Dunyi, L., Armstrong, R., 2011. Long-lived Paleoproterozoic granitic magmatism in the Seridó-Jaguaribe domain, Borborema Province-NE Brazil. J. South Am. Earth Sci. 32 (4), 287–300. https://doi.org/10.1016/j.jsames.2011.02.008.

Hollocher, K., Robinson, P., Walsh, E., Roberts, D., 2012. Geochemistry of amphibolite-facies volcanics and gabbros of the støren nappe in extensions west and southwest of Trondheim, Western Gneiss Region, Norway: a key to correlations and paleotectonic settings. Am. J. Sci. 312, 357–416. https://doi.org/10.2475/04.2012.01.

Irvine, T.N., Baragar, W.R.A., 1971. A guide to the chemical classification of the common volcanic rocks. Can. J. Earth Sci. 8, 523–548. https://doi.org/10.1139/e71-055.

Jackson, S.E., Pearson, N.J., Griffin, W.L., Belousova, E.A., 2004. The application of laserablation-inductively coupled plasma-mass spectrometry to in situ U-Pb zircongeochronology. Chem. Geol. 211, 47–69. https://doi.org/10.1016/j.chemgeo.2004.06.017.

Klein, E.L., Moura, C.A.V., 2008. São Luís Craton and Gurupi belt (Brazil): possible links with the West African Craton and surrounding Pan-African belts. Geol. Soc. Lond. Spec. Publ. 294, 137–151. https://doi.org/10.1144/SP294.8.

Klein, E.L., Lopes, E.C.S., Rodrigues, J.B., Souza-Gaia, S.M., Cordani, U.G., 2020. Rhyacian and Neoproterozoic magmatic associations of the Gurupi Belt, Brazil: implications for the tectonic evolution, and regional correlations. Geosci. Front. 11, 2243–2269. https://doi.org/10.1016/j.gsf.2020.02.016.

Klemme, S., Prowatke, S., Hametner, K., Günther, D., 2005. Partitioning of trace elements between rutile and silicate melts: implications for subduction zones. Geochim. Cosmochim. Acta 9, 2361–23711. https://doi.org/10.1016/j.gca.2004.11.015.

Lages, G.A., Santos, L.C.M.L., Brasilino, R.G., Rodrigues, J.B., Dantas, E.L., 2019. Statherian-Calymmian (ca. 1.6 Ga) magmatism in the Alto Moxotó Terrane, Borborema Province, Northeast Brazil: implications for within-plate and coeval collisional tectonics in West Gondwana. J. South Am. Earth Sci. 91, 116–130. https://doi.org/10.1016/j.jsames.2019.02.003.

Laurent, O., Martin, H., Moyen, J.F., Doucelance, R., 2014. The diversity and evolution of late-Archean granitoids: evidence for the onset of "modern-style" plate tectonics between 3.0 and 2.5 Ga. Lithos 205, 28–235. https://doi.org/10.1016/j.lithos.2014.06.012.

Lima, H.M., Pimentel, M.M., Fuck, R.A., Santos, L.C.M.L., Dantas, E.L., 2018. Geochemical and detrital zircon geochronological investigation of the metavolcanosedimentary Araticum complex, sergipano fold belt: implications for the evolution of the Borborema Province, NE Brazil. J. South Am. Earth Sci. 86, 176–192. https://doi.org/10.1016/j.jsames.2018.06.013.

Lima, H.M., Pimentel, M.M., Santos, L.C.M.L., Dantas, E.L., 2019. Isotopic and geochemical characterization of the metavolcano-sedimentary rocks of the Jirau do Ponciano Dome: a structural window to a Paleoproterozoic continental arc. Root within the Southern Borborema province, Northeast Brazil. J. South Am. Earth Sci. 90, 54–69. https://doi.org/10.1016/j.jsames.2018.12.002.

Ludwig, K.R., 2012. Isoplot 3.75: A geochronological toolkit for Microsoft Excel, Spec. Publ., no. 5. Berkeley Geochronology Center, Berkeley, California. 75p.

Lugmair, G.W., Marti, K., 1978. Lunar initial 143Nd/144Nd: differential evolution ofthe lunar crust and mantle. Earth Planet. Sci. Lett. 39, 349–357. https://doi.org/10.1016/0012-821X(78)90021-3.

Maniar, P.D., Piccoli, P.M., 1989. Tectonic discrimination of granitoids. Geol. Soc. Am. Bull. 101, 635–643. https://doi.org/10.1130/0016-7606(1989)101<0635:TDOG>2.3.CO;2.

Matteini, M., Junges, S.L., Dantas, E.L., Pimentel, M.M., Bühn, B.M., 2010. In situ zircon U-Pb and Lu-Hf isotope systematic on magmatic rocks: insights on the crustal evolution of the Neoproterozoic Goiás Magmatic Arc, Brasília Belt, Central Brazil. Gondwana Res. 16, 200–212 https://10.1016/j.gr.2009.05.008.

McDonough, W.F., Sun, S.s., 1995. The composition of the Earth. Chem. Geol. 120, 223–253. https://doi.org/10.1016/0009-2541(94)00140-4.

McMillan, N.J., Harmon, R.S., Moorbath, S., Lopez-Escobar, L., Strong, D.F., 1989. Crustal sources involved in continental arc magmatism: a case study of volcan Mocho-Choshuenco, southern Chile. Geology 17, 1152–1156. https://doi.org/10.1130/0091-7613(1989)017<1152:CSIICA>2.3.CO;2.

Meert, J.G., Santosh, M., 2017. The Columbia supercontinent revisited. Gondwana Res. 50, 67–83. https://doi.org/10.1016/j.gr.2017.04.011.

Miller, B.V., Coleman, D.S., 1988. Neodymium Isotope Geochemistry. Springer-Verlag. https://doi.org/10.1007/978-3-642-48916-7.

Nakamura, N., 1974. Determination of REE, Ba, Fe, Mg, Na and K in carbonaceous and ordinary chondrites. Geochim. Cosmochim. Acta 38 (5), 757–775. https://doi.org/10.1016/0016-7037(74)90149-5.

Neves, S.P., 2015. Constraints from zircon geochronology on the tectonic evolution of the Borborema Province (NE Brazil): widespread intracontinental Neoproterozoic reworking of a Paleoproterozoic accretionary orogen. J. South Am. Earth Sci. 58, 150–164. https://doi.org/10.1016/j.jsames.2014.08.004.

Neves, S.P., Lages, G.A., Brasilino, R.G., Miranda, A.W.A., 2015. Paleoproterozoic accretionary and collisional processes and the build-up of the Borborema Province (NE Brazil): geochronological and geochemical evidence from the Central Domain. J. South Am. Earth Sci. 58, 165–187. https://doi.org/10.1016/j.jsames.2014.06.009.

Neves, S.P., da Silva, J.M.R., Bruguier, O., 2017. Geometry, kinematics and geochronology of the Sertânia complex (Central Borborema Province, NE Brazil): assessing the role of accretionary versus intraplate processes during West Gondwana assembly. Precambrian Res. 298, 552–571. https://doi.org/10.1016/j.precamres.2017.07.006.

Oliveira, R.G., Medeiros, W.E., 2018. Deep crustal framework of the Borborema Province, NE Brazil, derived from gravity and magnetic data. Precambrian Res. 315, 45–65. https://doi.org/10.1016/j.precamres.2018.07.004.

Padilha, A.L., Vitorello, Í., Pádua, M.B., Fuck, R.A., 2016. Deep magnetotelluric signatures of the early Neoproterozoic Cariris Velhos tectonic event within the Transversal sub-province of the Borborema Province, NE Brazil. Precambrian Res. 275, 70–83. https://doi.org/10.1016/j.precamres.2015.12.012.

Pearce, J.A., 2014. Immobile element fingerprinting of ophiolites. Elements 10, 101–108. https://doi.org/10.2113/gselements.10.2.101.

Pearce, J.A., Harris, N.B.W., Tindle, A.G., 1984. Trace element discrimination diagrams for the tectonic interpretation of granitic rocks. J. Petrol. 25, 956–983. https://doi.org/10.1093/petrology/25.4.956.

Pedreira, A.J., De Waele, B., 2008. Contemporaneous evolution of the palaeoproterozoic mesoproterozoic sedimentary basins of the São Francisco-Congo craton. Geol. Soc. Spec. Publ. 294, 33. https://doi.org/10.1144/SP294.3.

Penaye, J., Toteu, S.F., Tchameni, R., Van Schmus, W.R., Tchakounté, J., Ganwa, A., Minyem, D., Nsifa, E.N., 2004. The 2.1 Ga West Central African belt in Cameroon: extension and evolution. J. Afr. Earth Sci. 39, 159–164. https://doi.org/10.1016/j.jafrearsci.2004.07.053.

Prouteau, G., Scaillet, B., Pichavant, M., 2001. Evidence for mantle metasomatism by hydrous silicic melts derived from subducted oceanic crust. Nature 410, 197–200. https://doi.org/10.1038/35065583.

Reddy, S.M., Evans, D.A.D., 2009. Palaeoproterozoic supercontinents and global evolution: correlations from core to atmosphere. Geol. Soc. Spec. Publ. 323, 1–26. https://doi.org/10.1144/SP323.1.

Sá, J.M., Sousa, L.C., Legrand, J.M., Galindo, A.C., Maia, H.N., Fillipi, R.R., 2014. U-Pb e Sm-Nd em ortognaisses Riacianos e Estaterianos nos Terrenos Rio Piranhas-Serido e Jaguaribeano, Província Borborema, Brasil. Geol. USP - Série Cient. 14, 97–110. https://doi.org/10.5327/Z1519-874X201400030007 (in Portuguese).

Santos, E.J., 1995. O complexo granítico Lagoa das Pedras: acresção e colisão na região de Floresta (Pernambuco), Província Borborema PhD thesis. Universidade de São Paulo, p. 228 (in Portuguese).

Santos, E.J., Medeiros, V.C., 1999. Constraints from granitic plutonism on Proterozoic crustal growth of the transverse zone, Borborema Province, NE Brazil. Rev. Bra. de Geoc 29, 73–84. https://doi.org/10.25249/0375-7536.1999297384.

Santos, E.J., Santos, L.C.M.L., 2019. Reappraisal of the Sumé complex: geochemistry and geochronology of metaigneous rocks and implications for Paleoproterozoic subduction-accretion events in the Borborema Province, NE Brazil. Braz. J. Geol. 49, (1). https://doi.org/10.1590/2317-4889201920180083 e20180083.

Santos, E.J., Nutman, A.P., Brito Neves, B.B., 2004. Idades SHRIMP U-Pb do Complexo Sertânia: implicações sobre a evolução tectônica da Zona Transversal, Província Borborema. Geol. USP. Série Cient. 4, 1–12. https://doi.org/10.5327/s1519-874x2004000100001 (in Portuguese).

Santos, T.J.S., Fetter, A.H., Neto, J.A.N., 2008. Comparisons between the northwestern Borborema Province, NE Brazil, and the southwestern Pharusian Dahomey Belt, SW Central Africa. Geol. Soc. Spec. Publ. 294, 101–120. https://doi.org/10.1144/SP294.6.

Santos, E.J., Van Schmus, W.R., Kozuch, M., de Neves, B.B.B., 2010. The Cariris Velhos tectonic event in Northeast Brazil. J. South Am. Earth Sci. 29, 61–76. https://doi.org/10.1016/j.jsames.2009.07.003.

Santos, L.C.M.L., Santos, E.J., Dantas, E.L., Lima, H.M., 2012. Análise estrutural e metamórfica da região de Sucuru (Paraíba): implicações sobre a evolução do Terreno Alto Moxotó, Província Borborema. Geol. USP - Série Cient. 12, 5–20. https://doi.org/10.5327/Z1519-874X2012000300001 (in Portuguese).

Santos, E.J., Souza Neto, J.A., Carmona, L.C.M., Armstrong, R., Santos, L.C.M.L., Mendes, L.U.D.S., 2013a. The metacarbonate rocks of Itatuba (Paraíba): a record of sedimentary recycling in a Paleoproterozoic collision zone of the Borborema province, NE Brazil. Precambrian Res. 23, 380–389. https://doi.org/10.1016/j.precamres.2012.09.021.

Santos, R.V., Santos, E.J., Neto, J.A.S., Carmona, L.C.M., Sial, A.N., Mancini, L.H., Santos, L.C.M.L., Nascimento, G.H., Mendes, L.U.S., Anastácio, E.M.F., 2013b. Isotope geochemistry of Paleoproterozoic metacarbonates from Itatuba, Borborema Province, Northeastern Brazil: evidence of marble melting within a collisional suture. Gondwana Res. 23, 380–389. https://doi.org/10.1016/j.gr.2012.04.010.

Santos, L.C.M.L., Dantas, E.L., Santos, E.J., Santos, R.V., Lima, H.M., 2015. Early to late Paleoproterozoic magmatism in NE Brazil: the Alto Moxotó Terrane and its tectonic implications for the pre-West Gondwana assembly. J. South Am. Earth Sci. 58, 188–209. https://doi.org/10.1016/j.jsames.2014.07.006.

Santos, T.J.S., Amaral, W.S., Ancelmi, M.F., Pitarello, M.Z., Fuck, R.A., Dantas, E.L., 2015a. U-Pb age of the coesite-bearing eclogite from NW Borborema Province, NE Brazil: implications for West Gondwana assembly. Gondwana Res. 28, 1183–1196. https://doi.org/10.1016/j.gr.2014.09.013.

Santos, L.C.M.L., Dantas, E.L., Cawood, P.A., Santos, E.J., Fuck, R.A., 2017a. Neoarchean crustal growth and Paleoproterozoic reworking in the Borborema Province, NE Brazil: insights from geochemical and isotopic data of TTG and metagranitic rocks of the Alto Moxotó Terrane. J. S. Am. Earth Sci. 79, 342–363. https://doi.org/10.1016/j.jsames.2017.08.013.

Santos, L.C.M.L., Dantas, E.L., Vidotti, R.M., Cawood, P.A., dos Santos, E.J., Fuck, R.A., Lima, H.M., 2017b. Two-stage terrane assembly in West Gondwana: insights from structural geology and geophysical data of Central Borborema Province, NE Brazil. J. Struct. Geol. 103, 167–184. https://doi.org/10.1016/j.jsg.2017.09.012.

Santos, L.C.M.L., Dantas, E.L., Cawood, P.A., Lages, G.A., Lima, H.M., Santos, E.J., 2018. Accretion Tectonics in Western Gondwana deduced from Sm-Nd Isotope mapping of terranes in the Borborema Province, NE Brazil. Tectonics 37, 2727–2743. https://doi.org/10.1029/2018TC005130.

Santos, L.C.M.L., Dantas, E.L., Cawood, P.A., de Lages, G.A., Lima, H.M., dos Santos, E.J., Caxito, F.A., 2019. Early to late Neoproterozoic subduction-accretion episodes in the Cariris Velhos Belt of the Borborema Province, Brazil: insights from isotope and whole-rock geochemical data of supracrustal and granitic rocks. J. South Am. Earth Sci. 96, 102384. https://doi.org/10.1016/j.jsames.2019.102384.

Santos, L.C.M.L., Lima, H.M., Lages, G.A., Caxito, F.A., Araújo Neto, J.F., Guimarães, I.P., 2020. Petrogenesis of the Riacho do Icó Stock: evidence for Neoproterozoic slab melting during accretion tectonics in the Borborema Province? Braz. J. Geol. 50, (1). https://doi.org/10.1590/2317-4889202020190127 e20190127.

Shaw, S.E., Flood, R.H., 1981. The New England Batholith, eastern Australia: geochemical variations in time and space. J. Geophys. Res. 86, 530–10,544 https://10.1029/JB086iB11p10530.

Sial, A.N., Ferreira, V.P., 2016. Magma associations in Ediacaran granitoids of the Cachoeirinha–Salgueiro and Alto Pajeú terranes, northeastern Brazil: forty years of studies. J. South Am. Earth Sci. 68, 113–133. https://doi.org/10.1016/j.jsames.2015.10.005.

Souza, Z.S., Martin, H., Peucat, J.J., Jardim De Sá, E.F., De Freitas Macedo, M.H., 2007. Calc-alkaline magmatism at the Archean-Proterozoic transition: the Caicó

complex Basement (NE Brazil). J. Petrol. 48, 2149–2185. https://doi.org/10.1093/petrology/egm055.
Tatsumi, Y., Stern, R.J., 2006. Manufacturing continental crust in the subduction factory. Oceanography 19. https://doi.org/10.5670/oceanog.2006.09. 114–112.
Toteu, S.F., Van Schmus, W.R., Penaye, J., Michard, A., 2001. New U-Pb and Sm-Nd data from north-Central Cameroon and its bearing on the pre-Pan African history of Central Africa. Precambrian Res. 1-8, 45–73. https://doi.org/10.1016/S0301-9268(00)00149-2.
Tsoungui, P.N.E., Ganno, S., Njiosseu, E.L.T., Mbongue, J.L.N., Woguia, B.K., Tamehe, L. S., Wambo, J.D.T., Nzenti, J.P., 2020. Geochemical constraints on the origin and tectonic setting of the serpentinized peridotites from the Paleoproterozoic Nyong series, Eseka area, SW Cameroon. Acta Geoch. 39, 404–422. https://doi.org/10.1007/s11631-019-00368-4.
Van Schmus, W.R., Brito Neves, B.B., Hackspacher, P., Babinski, M., 1995. U Pb and Sm Nd geochronologic studies of the eastern Borborema Province, Northeastern Brazil: initial conclusions. J. South Am. Earth Sci. 8, 267–288. https://doi.org/10.1016/0895-9811(95)00013-6.
Van Schmus, W.R., Brito Neves, B.B., Williams, I.S., Hackspacher, P.C., Fetter, A.H., Dantas, E.L., Babinski, M., 2003. The Seridó group of NE Brazil, a late neoproterozoic pre- to syn-collisional basin in West Gondwana: insights from SHRIMP U-Pb detrital zircon ages and Sm-Nd crustal residence (TDM) ages. Precambrian Res. 127, 287–327. https://doi.org/10.1016/S0301-9268(03)00197-9.
Van Schmus, W.R., Oliveira, E.P., Silva Filho, A.F., Toteu, S.F., Penaye, J., Guimarães, I. P., 2008. Proterozoic links between the Borborema Province, NE Brazil, and the Central African fold belt. Geol. Soc. Spec. Publ. https://doi.org/10.1144/SP294.5.
Wiedenbeck, M., Hanchar, J.M., Peck, W.H., Sylvester, P., Valley, J., Whitehouse, M., Kronz, A., Morishita, Y., Nasdala, L., Fiebig, J., Franchi, I., Girard, J.-P., Greenwood, R.C., Hinton, R., Kita, N., Mason, P.R.D., Norman, M., Ogasawara, M., Piccoli, P.M., Rhede, D., Satoh, H., Schulz-Dobrick, B., Skår, Ø., Spicuzza, M.J., Terada, K., Tindle, A., Togashi, S., Vennemann, T., Xie, Q., Zheng, Y.-F., 2004. Further characterisation of the 91500 zircon crystal. Geostand. Geoanal. Res. 28, 9–39. https://doi.org/10.1111/j.1751-908X.2004.tb01041.x.
Wood, D.A., 1980. The application of a Th–Hf–Ta diagram to problems of tectonomagmatic classification and to establishing the nature of crustal contamination of basaltic lavas of the British Tertiary Volcanic Province. Earth Planet. Sci. Lett. 50, 11–30. https://doi.org/10.1016/0012-821X(80)90116-8.
Xia, Y., Xu, X., 2019. A fragment of Columbia supercontinent: insight for Cathaysia block basement from tectono-magmatic evolution and mantle heterogeneity. Geophys. Res. Lett. 46, 2012–2024. https://doi.org/10.1029/2018GL081882.
Zhao, G., Cawood, P.A., Wilde, S.A., Sun, M., 2002. Review of global 2.1-1.8 Ga orogens: implications for a pre-Rodinia supercontinent. Earth Sci. Rev. 59, 125–162. https://doi.org/10.1016/S0012-8252(02)00073-9.
Zhao, G., Sun, M., Wilde, S.A., Li, S., 2004. A Paleo-Mesoproterozoic supercontinent: assembly, growth and breakup. Earth Sci. Rev. 67, 91–123. https://doi.org/10.1016/j.earscirev.2004.02.003.